

國立交通大學

光電工程研究所

碩士論文

熱極化二階非線性光纖特性之研究

A study on the second-order optical nonlinearity of thermally poled
optical fibers



研究生：吳金水

指導教授：賴暎杰 博士

中華民國九十四年七月

熱極化二階非線性光纖特性之研究

A study on the second-order optical nonlinearity of thermally poled
optical fibers

研究生: 吳金水

Student: Ng Kam Sooi (Jimmy Ng)

指導教授: 賴暎杰 博士

Advisor: Dr. Yinchieh Lai

國立交通大學



A Thesis

Submitted to Department of Photonics & Institute of Electro-Optical Engineering

College of Electrical Engineering and Computer Science

National Chiao Tung University

In Partial Fulfillment of Requirements for the Degree of

Master in Electro-Optical Engineering

July 2005

Hsinchu, Taiwan, Republic of China

中華民國九十四年七月

A study on the second-order optical nonlinearity of thermally poled optical fibers

Student: Ng Kam Sooi(Jimmy Ng)

Advisor: Dr. Yinchieh Lai

Institute of Electro-optical engineering

College of Electrical Engineering and Computer Science

National Chiao Tung University



Silica glass is an important material in optoelectronics because of its low transmission loss, low fabrication cost, high optical damage threshold and possible optical fiber compatibility. However, silica glass is also a material with macroscopic inversion symmetry, which means that it does not exhibit second-order nonlinearity. In this thesis study we investigate how to achieve second-order nonlinearity in silica glass D-shape optical fibers by means of the thermal poling method. Second harmonic generation from 1064nm to 532nm is observed in our preliminary experiments.

熱極化二階非線性光纖特性之研究

研究生：吳金水

指導老師：賴暎杰 博士

國立交通大學光電工程研究所

摘要

矽玻璃因具有低損耗、便宜、耐高強度光、和可能與光纖相容等優點，使它成為光電子領域中主要的應用物質。不過因為矽玻璃具反轉對稱性，故無二階非線性光學特性。在本論文中我們研究如何利用熱極化的方法來在 D-shape 光纖中產生二階非線性效應，也在初步的實驗中成功地觀測到由 1064 nm 波長的入射光轉換成 532 nm 波長光的二次倍頻現象。

Acknowledgement

不知不覺又到了畢業的季節，在這兩年裡讓我深深地感受到做實驗的樂趣。在此要衷心的感謝賴老師的教誨，讓我在這兩年中學到了很多東西。在實驗上，非常感謝項維巍學長陪伴我做實驗，對於實驗的架設與分析也不厭其煩一一為我解答，另外也要感謝徐桂珠學姐在實驗上的協助。還有特別要感謝孔慶昌老師提供了一個實驗場所和在實驗儀器的商借，這才能讓我順利的完成實驗。

感謝實驗室的同學吳銘峰(峰哥)、林倩仔(阿桑)和張淑惠(阿姐)陪我一起度過這兩年的時光，在課業上一起討論，在實驗上互相勉勵，在球場上一起的嘶拼，讓我充實愉快地度過我碩士的兩年生活，尤其要感謝阿姐肯隨時抽空協助我們的實驗。感謝實驗室的學弟們在實驗室帶來的熱鬧氣氛，讓我們更有活力地繼續我們的實驗。還有也要感謝祁老師、陳老師和馮老師的學生在實驗室裡帶來無限的歡樂(“十分”的遊戲)。最後，也要感謝原分所的助理與學生小裴(Charles)、Alan 和 Erika，在實驗上的協助與討論。

感謝我的父母和哥哥姐姐的鼓勵與支持，最後要非常感謝我的女朋友淑娟，在這些日子裡的陪伴與支持，讓我覺得人生充滿著希望。

Table of contents

English abstract	I
Chinese abstract	II
Acknowledgement	III
Contents	IV
Diagram contents	VI
CHAPTER 1 Introduction	1
1.1 History of second-order nonlinearity in optical fibers	1
1.2 Motivation of the research	3
1.3 Organization of the thesis	3
CHAPTER 2 Basic concept of second-harmonic generation on optical fibers	5
2.1 Principle of nonlinear optics	5
2.1.1 Nonlinear susceptibility	7
2.1.2 Tensor	8
2.1.3 Coupled wave equation	10
2.1.4 Second-harmonic generation	12
2.1.5 Quasi-phase matching	13
2.2 Quasi-phase-matched second harmonic generation in periodically poled fibers ...	18
2.3 Mechanism of thermal poling	20



2.4	Mechanism of ultraviolet erasure	26
CHAPTER 3	Experimental procedures and results	27
3.1	Introduction	27
3.2	D-shaped optical fiber	27
3.3	Experimental procedures	28
3.3.1	D-shaped fibers etching	29
3.3.2	Thermal poling	30
3.3.3	Second-harmonic generation measurement	31
3.3.4	Ultraviolet erasure	32
3.4	Results and conclusion	35
3.4.1	Thermally poled fused silica plate	35
3.4.2	Pump power dependence for second-harmonic power	38
3.4.3	Polarization dependence for second-harmonic power	39
3.4.4	Estimation of d_{33}	40
3.4.5	UV erasure and UV periodic grating	40
CHAPTER 4	Conclusions	42
4.1	Summary of results	42
4.2	Future work	42
References	44



Diagram contents

Fig. 2.1(a)	Energy-level, conservation of energy	6
Fig. 2.1(b)	Momentum vectors, conservation of momentum	6
Fig. 2.2	Sum-frequency generation, where d is the second-order nonlinear coefficient and $\chi^{(2)}$ is the second-order nonlinear susceptibility ...	7
Fig. 2.3	Second-harmonic generation	13
Fig. 2.4	$\sin c^2(\frac{\Delta kL}{2})$ vs $\frac{\Delta kL}{2}$	14
Fig. 2.5(a)	First-order quasi-phase matching of ferroelectric crystal	17
Fig. 2.5(b)	First-order quasi-phase matching of thermally poled silica fiber	18
Fig. 2.6	Formation process of the depletion region near the anode surface of the thermally poled fused silica	24
Fig. 2.7(a)	Planar schematic diagram of fused silica network before poling	25
Fig. 2.7(b)	Planar schematic diagram of fused silica network after poling	25
Fig. 3.1	D-shape fiber	28
Table 3.1	The parameters of the D-shape fibers	28
Fig. 3.2	Ecthed D-shape fiber	29
Fig. 3.3	The diagram of the thermal poling system	31
Fig. 3.4	SH signal vs poling time at $280^{\circ}C$, in Ref. [18]	31
Fig. 3.5	SH measurement experimental setup	32
Fig. 3.6	Experimental setup of UV erasure system	34
Fig. 3.7	Experimental setup of UV periodic grating	34
Table 3.2	Quasi- phase matching period for fused silica with difference mol% of doped GeO_2	35
Fig. 3.8	The diagram of thermally poled fused silica plate	36

Fig. 3.9(a)	The surface of the etched thermally poled fused silica plate viewed under an optical microscope	37
Fig. 3.9(b)	The surface of the etched thermally poled fused silica plate viewed under AFM scanning	37
Fig. 3.10	SH power vs fundamental power for $S \rightarrow S$ and $P \rightarrow S$ conversion	38
Fig. 3.11	SH power vs tuning angle of half-wave plate	39



Chapter 1 Introduction

1.1 History of second-order nonlinearity in optical fibers

In 1986, Osterberg and Margulis reported the first second-harmonic generation (SHG) in a Ge-doped single mode fiber irradiated by a CW 1064 nm Q-switched and mode-locked Nd:YAG laser [1]. At first, it was just a very weak green light output from the end of the optical fiber. After a few hours, the green light intensity was increasing exponentially with the irradiated time and was saturated after 12 hours irradiation. The second-harmonic (SH) conversion efficiency could be as high as 5%. This is the first discovery that self-organized growth of green second harmonic light can be observed in optical fibers with infrared light input. The next year, 1987, Stolen and Tom generated SH lights from a Ge-doped single-mode fiber after a few minutes of seeding with 532nm harmonic lights along with the 1064nm fundamental lights [2]. After seeding for 5 minutes and then removing the seeding source, it was found that one can still see the green output lights from the end of the fiber. These experiments suggest that there is a mechanism that can break the inversion symmetry of silica materials and can produce a self-organized $\chi^{(2)}$ grating that is automatically phase-matched to the input lights.

In 1988, Bergot et al. observed large permanent enhancement in the second-order optical nonlinearity of silica materials by applying of a transverse dc electric poling field in the presence of high-intensity lights [3]. The external dc electric poling field has an effect on the

defects, similar to that of the internal light field in previous experiments. Because of the applied external fields can be 5 orders of magnitude larger than the light fields, it can be more effective. Significant frequency doubling occurs despite the absence of the phase matching. The SH signals grow quadratically with the poling field, and above $\sim 4\text{V}/\mu\text{m}$ they get saturated.

After 3 years, in 1991 Myers et al. found that large and stable second-order nonlinear susceptibility approaching 1 pm/V could be created in fused silica by means of the thermal poling technique [4]. The thermal poling condition was performed at $250\text{-}325^\circ\text{C}$ under an applied electrical field, and the second-order nonlinearity appears in a thin layer of fused silica plate just under the anode. Since 1991, second-order nonlinearities in the order of 1 pm/V have been achieved in glasses by a variety of different techniques including thermal poling [4], corona poling [5], and electron implantation [6].

In 1999 Pruneri et al. [7] fabricated second-order nonlinear gratings in D-shape germanosilicate fibers by thermal poling with periodic electrodes defined by standard photolithography. The grating length is 75 mm long and it is suitable for the quasi-phase-matched (QPM) frequency doubling of $1.532\ \mu\text{m}$ lights. The SH power was 6.8 mW and the SH peak power greater than 1.2 kW at 766 nm was generated, in which the average and peak conversion efficiencies are as high as 21% and 30% , respectively.

The second-order nonlinearity in poled fused silica can be erased by heating [2], electron

beam [8], ultraviolet (UV) [9,10], or near infrared (NIR) [11]. These mechanisms can be used to implement quasi-phase-matched SHG. In 2000, Bonfrate et al. exposed UV lights through a periodic amplitude mask to a uniformly poled fiber and successfully demonstrated periodic UV erasure of second-order nonlinearity for achieving quasi-phase-matched SHG in optical fibers [12]. However, the second-order nonlinearity generation mechanism in glasses still remains not to be identified completely.

1.2 Motivation of the research

Second-order nonlinearity in optical fibers can be used to develop linear electrooptic modulation, switching, and parametric frequency conversion. The thermally poled optical fibers offer larger bandwidth and low group-velocity mismatch, and therefore the relatively low value of the nonlinear coefficient (compared with polar crystals waveguide, such as lithium niobate, potassium titanyl phosphate) can be compensated for by an increase in the length of the fiber so that it is suitable for the pulsed frequency conversion.

1.3 Organization of the thesis

The thesis consists of four chapters. Chapter 1 gives an introduction of the second-order nonlinearity in optical fibers and explains our motivation for doing this research. Chapter 2 describes the basic concept of SHG, and the mechanisms of thermal poling and UV erasure in

optical fibers. Chapter 3 presents the experiment procedures and results. In Chapter 4 we make a brief conclusion and discuss possible future research directions.



Chapter 2 Basic concept of second-harmonic generation in optical fibers

2.1 Principle of nonlinear optics

The first working laser was made by Theodore H. Maiman in 1960 [13]. He used a solid-state flash-lamp-pumped ruby crystal to produce red laser lights at 694nm. The invention of the laser enabled us to examine the behavior of lights in optical materials at higher intensities. In fact, the beginning of the field of nonlinear optics is often taken to be the discovery of SHG by Franken et al. in 1961 [14].

Nonlinear optics is the study of phenomena that occur as a consequence of the modification of the optical properties of a material system by the presence of lights [15, 16]. They occur when the response of a material system to an applied optical field depends on a nonlinear manner upon the strength of the optical field, and the intense laser field can cause the polarization of the medium to develop new frequency components that are not present in the incident field. These new frequency components of the polarization act as sources of new frequency components of the electromagnetic field.

The nonlinear processes also have to satisfy the conditions of conservation of energy and conservation of momentum, in order to get the optimum conversion efficiency. Fig. 2.1 illustrates the relation between the energy-level and the momentum vectors.

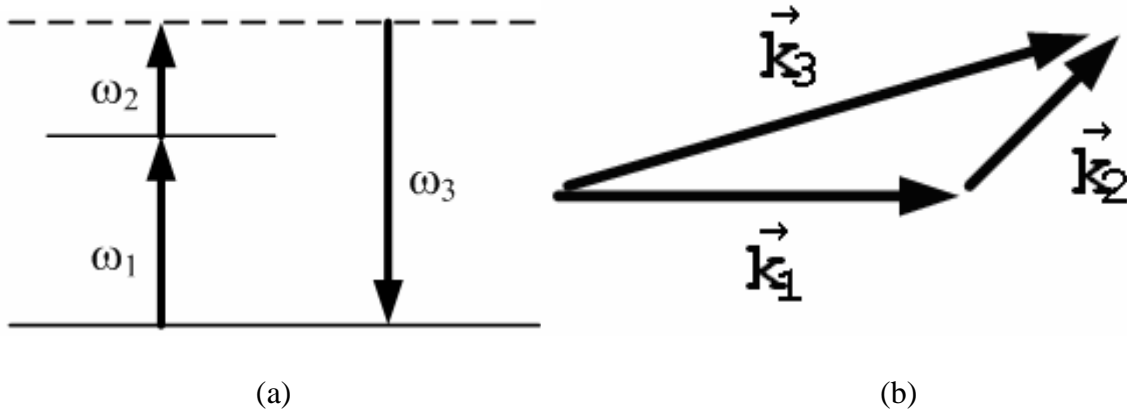


Fig. 2.1 (a) Energy-level, conservation of energy ($\hbar\omega_1 + \hbar\omega_2 = \hbar\omega_3$),

Fig. 2.1 (b) Momentum vectors, conservation of momentum ($\hbar\vec{k}_1 + \hbar\vec{k}_2 = \hbar\vec{k}_3$).

As an example of nonlinear optical interaction, let us consider the process of sum-frequency generation, which is illustrated schematically in Fig. 2.2. A weak light (ω_1) and an intense pump light (ω_2) are incident into a nonlinear medium simultaneously. After the sum frequency generation process, a light (ω_3) which frequency is the sum of ω_1 and ω_2 , emits from the nonlinear medium.

$$\omega_3 = \omega_1 + \omega_2 \quad (2.1)$$

This process is known as the up-conversion and equation (2.1) is the condition of conservation of energy.

On the other hand,

$$\Delta\vec{k} = \vec{k}_3 - \vec{k}_2 - \vec{k}_1 \quad (2.2)$$

is called the wave vector (or momentum) mismatch, which describes how good the phase

matching (momentum conservation) is achieved. If the process satisfy the phase matching condition ($\Delta k = 0$), it will be under the optimum working condition.

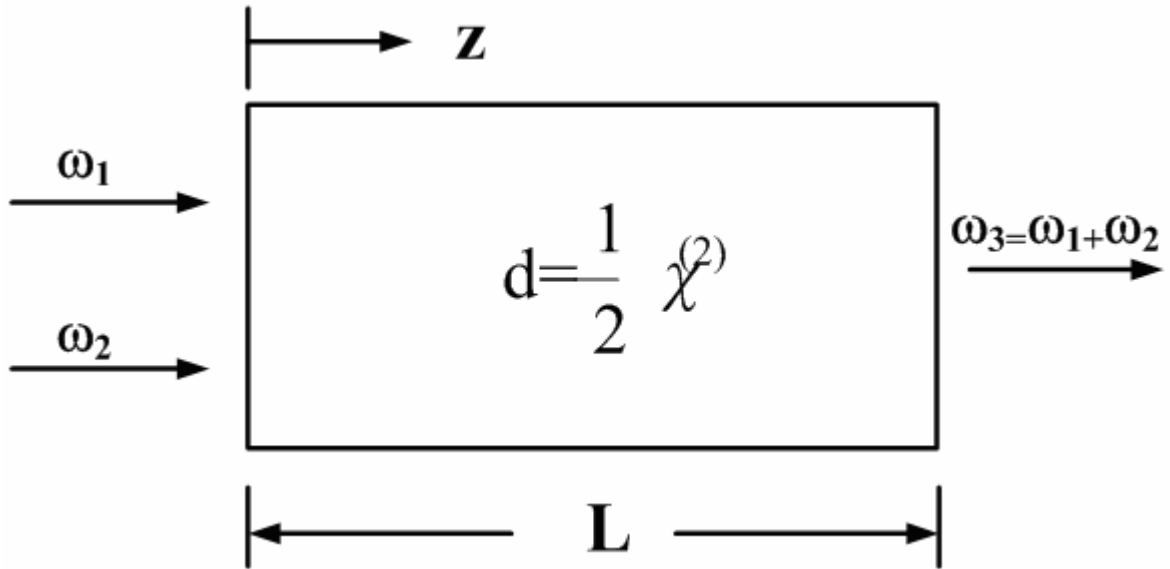


Fig. 2.2 Sum-frequency generation, where d is the second-order nonlinear coefficient and $\chi^{(2)}$ is the second-order nonlinear susceptibility.

2.1.1 Nonlinear susceptibility

A linear dielectric medium is characterized by a linear relation between the polarization (P) and the electric field (E),

$$P = \varepsilon_0 \chi^{(1)} E \quad (2.3)$$

where ε_0 is the permittivity of free space and $\chi^{(1)}$ is the linear electric susceptibility of the medium. The relation between the dielectric constant, refractive index and $\chi^{(1)}$ is as below,

$$n^2 = \frac{\varepsilon}{\varepsilon_0} = 1 + \chi^{(1)} \quad (2.4)$$

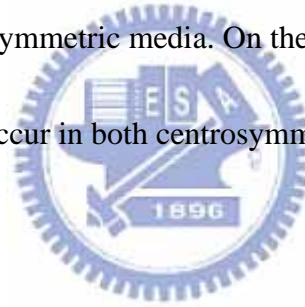
But in a nonlinear dielectric medium, the polarization can be a power series of the

electric field, which can be expressed as

$$P = \varepsilon_0[\chi^{(1)}E + \chi^{(2)}E^2 + \chi^{(3)}E^3 + \dots] \quad (2.5)$$

The first term, which is linear, dominates at small electric field E . The second term represents a quadratic effect, where $\chi^{(2)}$ is the second-order nonlinear susceptibility. The third term represents third-order nonlinearity and $\chi^{(3)}$ is the third-order nonlinear susceptibility. Actually the linear susceptibility $\chi^{(1)}$ is a second-rank tensor and the n -order nonlinear susceptibility $\chi^{(n)}$ is a $(n+1)^{\text{th}}$ - rank tensor.

The second-order nonlinear optical interaction can occur in a noncentrosymmetric media only. That is, they do not exist in symmetric media. On the other hand, the third-order nonlinear optical interaction can occur in both centrosymmetric and noncentrosymmetric media.



2.1.2 Tensor

In a noncentrosymmetric medium, we can describe the Cartesian components of the second-order nonlinear polarization density and the second-order nonlinear susceptibility as $P_i^{(2)}$ and χ_{ijk} , respectively, where i, j and k are the Cartesian coordinates x, y and z . We introduce the second-order susceptibility tensor

$$d_{ijk} = \frac{1}{2} \chi_{ijk} \quad (2.6)$$

For sum frequency generation,

$$P_i^{(2)} = \sum_{j,k} \sum_{m,n} \varepsilon_0 \chi_{ijk}^{(2)}(-(\omega_m + \omega_n); \omega_m, \omega_n) E_j(\omega_m) E_k(\omega_n) \quad (2.7)$$

and for second harmonic generation,

$$\begin{aligned} P_{i,2\omega}^{(2)}(2\omega) &= \sum_{j,k} \varepsilon_0 \chi_{ijk}^{(2)}(-2\omega; \omega, \omega) E_j(\omega_m) E_k(\omega_n) \\ &= 2 \sum_{j,k} \varepsilon_0 d_{ijk}(-2\omega; \omega, \omega) E_j(\omega) E_k(\omega) \end{aligned} \quad (2.8)$$

where E_j and E_k are the electric fields in y and z directions, respectively.

According to the Kleinman symmetry condition, the d_{ijk} is with the intrinsic permutation symmetry, where the last two indices j and k can be interchanged freely without altering the nonlinear susceptibility tensor, i.e. $d_{ijk} = d_{ikj}$. Therefore the following contracted

notation is used

jk	:	11	22	33	23,32	31,13	12,21
l	:	1	2	3	4	5	6



d_{ijk} can be defined as d_{il} and become a 3X6 matrix,

$$d_{il} = \begin{bmatrix} d_{11} & d_{12} & d_{13} & d_{14} & d_{15} & d_{16} \\ d_{21} & d_{22} & d_{23} & d_{24} & d_{25} & d_{26} \\ d_{31} & d_{32} & d_{33} & d_{34} & d_{35} & d_{36} \end{bmatrix} \quad (2.9)$$

For sum frequency generation,

$$\begin{bmatrix} P_x(\omega_3) \\ P_y(\omega_3) \\ P_z(\omega_3) \end{bmatrix} = 2\varepsilon_0 \begin{bmatrix} d_{11} & d_{12} & d_{13} & d_{14} & d_{15} & d_{16} \\ d_{21} & d_{22} & d_{23} & d_{24} & d_{25} & d_{26} \\ d_{31} & d_{32} & d_{33} & d_{34} & d_{35} & d_{36} \end{bmatrix} \begin{bmatrix} E_x(\omega_1)E_x(\omega_2) \\ E_y(\omega_1)E_y(\omega_2) \\ E_z(\omega_1)E_z(\omega_2) \\ E_y(\omega_1)E_z(\omega_2) + E_z(\omega_1)E_y(\omega_2) \\ E_x(\omega_1)E_z(\omega_2) + E_z(\omega_1)E_x(\omega_2) \\ E_x(\omega_1)E_y(\omega_2) + E_y(\omega_1)E_x(\omega_2) \end{bmatrix} \quad (2.10)$$

For SHG,

$$\begin{bmatrix} P_x(2\omega) \\ P_y(2\omega) \\ P_z(2\omega) \end{bmatrix} = 2\varepsilon_0 \begin{bmatrix} d_{11} & d_{12} & d_{13} & d_{14} & d_{15} & d_{16} \\ d_{21} & d_{22} & d_{23} & d_{24} & d_{25} & d_{26} \\ d_{31} & d_{32} & d_{33} & d_{34} & d_{35} & d_{36} \end{bmatrix} \begin{bmatrix} E_x(\omega)^2 \\ E_y(\omega)^2 \\ E_z(\omega)^2 \\ 2E_y(\omega)E_z(\omega) \\ 2E_x(\omega)E_z(\omega) \\ 2E_x(\omega)E_y(\omega) \end{bmatrix} \quad (2.11)$$

The material of our thermally poled optical fibers is fused silica, which the point group is ∞ mm and the interaction frequencies are far away from the absorption frequencies.

According to the Kleinman symmetry condition, the second-order susceptibility tensor is

$$d_{il} = \begin{bmatrix} 0 & 0 & 0 & 0 & d_{31} & 0 \\ 0 & 0 & 0 & d_{31} & 0 & 0 \\ d_{31} & d_{31} & d_{33} & 0 & 0 & 0 \end{bmatrix} \quad (2.12)$$

therefore the SHG of thermal-poled optical fibers is

$$\begin{bmatrix} P_x(2\omega) \\ P_y(2\omega) \\ P_z(2\omega) \end{bmatrix} = 2\varepsilon_0 \begin{bmatrix} 2d_{31}E_z(\omega)E_x(\omega) \\ 2d_{31}E_y(\omega)E_z(\omega) \\ d_{31}E_x(\omega)^2 + d_{31}E_y(\omega)^2 + d_{33}E_z(\omega)^2 \end{bmatrix} \quad (2.13)$$

Stolen and Tom [2] proposed that an effective $\chi^{(2)}$ originates from the interaction between the third-order susceptibility $\chi^{(3)}$ and a built-in static electrical field E_l , that is

$$\chi_{ijk}^{(2)}(-2\omega; \omega, \omega) = 3\chi_{ijkl}^{(3)}(-2\omega; \omega, \omega, 0)E_l \quad (2.14)$$

because $\chi_{3333}^{(3)} = 3\chi_{3113}^{(3)}$ for the centrosymmetric medium, therefore

$$d_{33} = 3d_{31} \quad (2.15)$$

2.1.3 Coupled wave equation

In a lossless and nonlinear medium, the propagation of lights can be described by

Maxwell's equations,

$$\begin{aligned}\nabla \times \vec{H} &= \frac{\partial \vec{D}}{\partial t} & \nabla \times \vec{H} &= 0 \\ \nabla \times \vec{E} &= -\mu_0 \frac{\partial \vec{H}}{\partial t} & \nabla \times \vec{D} &= 0\end{aligned}\quad (2.16)$$

where $\vec{D} = \varepsilon_0 \vec{E} + \vec{P}$

$$\begin{aligned}\vec{P} &= \vec{P}_L + \vec{P}_{NL} = \varepsilon_0 \chi^{(1)} \vec{E} + \vec{P}_{NL} \\ \vec{B} &= \mu_0 \vec{H}\end{aligned}\quad (2.17)$$

\vec{P}_{NL} is the nonlinear polarization vector.

$$\text{Because } \nabla \times \nabla \times \vec{E} = \nabla(\nabla \cdot \vec{E}) - \nabla^2 \vec{E}\quad (2.18)$$

$$\text{Therefore, } \nabla^2 \vec{E} = \mu_0 \left(\varepsilon \frac{\partial^2 \vec{E}}{\partial t^2} + \frac{\partial^2 \vec{P}_{NL}}{\partial t^2} \right)\quad (2.19)$$

where $\varepsilon = \varepsilon_0(1 + \chi^{(1)})$, equation (2.19) is the wave equation.

If we consider the sum frequency generation $\omega_3 = \omega_1 + \omega_2$, the total electric field can be represented as

$$\begin{aligned}\vec{E} &= \overline{E(\omega_1, z, t)} + \overline{E(\omega_2, z, t)} + \overline{E(\omega_3, z, t)} \\ &= \frac{1}{2} \sum_{j=1}^3 [E_j(z) e^{i(\omega_j t - k_j z)} + c.c.] \end{aligned}\quad (2.20)$$

According to the slowly varying envelope approximation (SVEA),

$$\left| k_j \frac{\partial E_j(z)}{\partial z} \right| \gg \left| \frac{\partial^2 E_j(z)}{\partial z^2} \right|\quad (2.21)$$

so $\frac{\partial^2 E_j(z)}{\partial z^2}$ can be neglected.

From equations (2.17) and (2.18), we get

$$\frac{\partial E_1(z)}{\partial z} = -\frac{i\omega_1}{2} \sqrt{\frac{\mu_0}{\varepsilon_1}} d_{eff} E_3(z) E_2^*(z) e^{i\Delta k z}\quad (2.22)$$

$$\frac{\partial E_2^*(z)}{\partial z} = \frac{i\omega_2}{2} \sqrt{\frac{\mu_0}{\epsilon_2}} d_{eff} E_1(z) E_3^*(z) e^{i\Delta k z} \quad (2.23)$$

$$\frac{\partial E_3(z)}{\partial z} = -\frac{i\omega_3}{2} \sqrt{\frac{\mu_0}{\epsilon_3}} d_{eff} E_1(z) E_2(z) e^{i\Delta k z} \quad (2.24)$$

where $\Delta k = k_3 - k_2 - k_1$ is the wave vector mismatch and $d_{eff} = \frac{1}{2} \chi_{eff}^{(2)}$ is the effective value of nonlinear coefficient. Equations (2.22), (2.23) and (2.24) are the coupled waves equations.

2.1.4 Second-harmonic generation

For SHG, if a wave propagating in the z direction with frequency $\omega = \omega_1 = \omega_2$ is normal incident into a lossless and nonlinear medium, its SH wave is with the frequency $\omega_3 = \omega_1 + \omega_2 = 2\omega$. Fig 2.3 shows the schematic of SHG. From equation (2.24), we have

$$\frac{\partial E_{2\omega}(z)}{\partial z} = -i\omega \sqrt{\frac{\mu_0}{\epsilon_{2\omega}}} d_{eff} [E_{2\omega}(z)]^2 e^{i\Delta k z} \quad (2.25)$$

$$\text{where } \Delta k = k_3 - 2k_1 = k_{2\omega} - 2k_\omega = \frac{4\pi}{\lambda_\omega} (n_{2\omega} - n_\omega) \quad (2.26)$$

In the undepleted-pump approximation, $E_\omega(z)$ is constant. If $E_\omega(0)=0$ is the initial condition, $E_{2\omega}(0)$ is equal to zero.

Therefore,

$$E_{2\omega}(L) = \int_{E_{2\omega}(0)=0}^{E_{2\omega}(L)} dE_{2\omega} = \int_0^L \frac{\partial E_{2\omega}(z)}{\partial z} dz = -i\omega \sqrt{\frac{\mu_0}{\epsilon_{2\omega}}} [E_{2\omega}(z)]^2 \int_0^L d_{eff} e^{i\Delta k z} dz \quad (2.27)$$

where L is the length of the medium.

We can express the SH power as

$$P_{2\omega} = \frac{1}{2} \sqrt{\frac{\epsilon_{2\omega}}{\mu_0}} |E_{2\omega}|^2 A$$

$$\begin{aligned}
&= 2 \left(\frac{\mu_0}{\epsilon_{2\omega}} \right)^{\frac{3}{2}} \frac{\omega^2}{n_\omega^2 n_{2\omega}} \frac{P_\omega^2}{A} \left| \int_0^L d_{\text{eff}} e^{i\Delta kz} dz \right|^2 \\
&= 2 \left(\frac{\mu_0}{\epsilon_{2\omega}} \right)^{\frac{3}{2}} \frac{\omega^2 d_{\text{eff}}^2 L^2}{n_\omega^2 n_{2\omega}} \frac{P_\omega^2}{A} \text{sinc}^2 \left(\frac{\Delta k L}{2} \right)
\end{aligned} \tag{2.28}$$

where $n_\omega = \sqrt{\frac{\epsilon_\omega}{\epsilon_0}}$, $n_{2\omega} = \sqrt{\frac{\epsilon_{2\omega}}{\epsilon_0}}$ and A is the beam-size of beam.

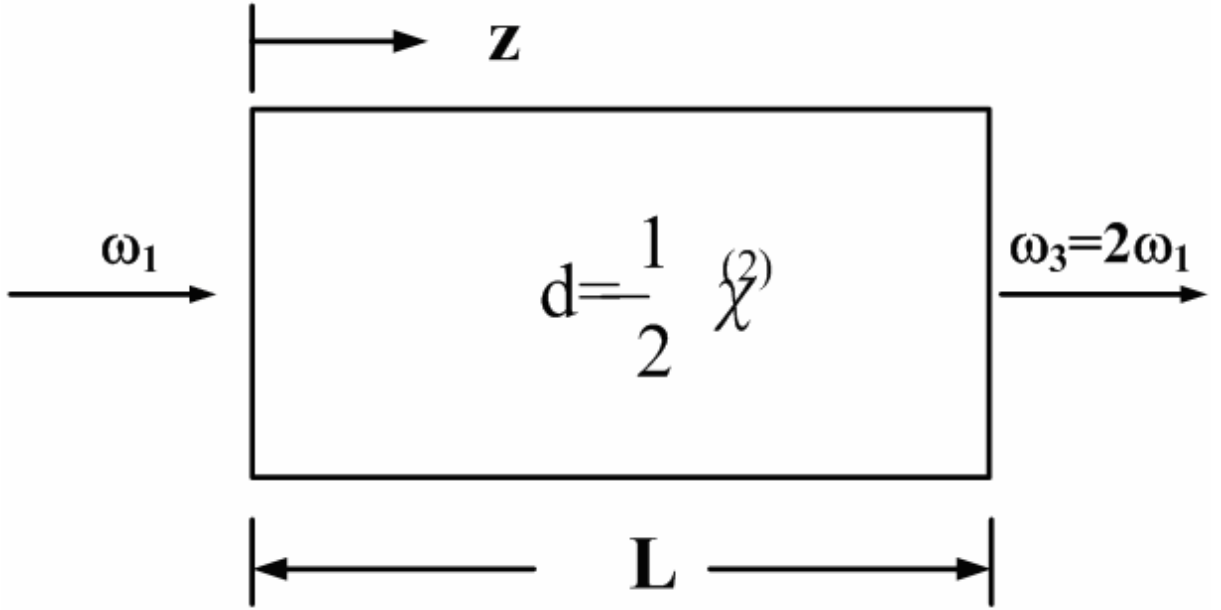


Fig. 2.3 Second-harmonic generation.

2.1.5 Quasi-phase matching

From equation (2.28), we observe that the SH power $P_{2\omega}$ is proportional to d_{eff}^2 , L^2 and $\text{sinc}^2(\frac{\Delta k L}{2})$, Fig. 2.4 shows the relation between $\text{sinc}^2(\frac{\Delta k L}{2})$ and $\frac{\Delta k L}{2}$. If the process satisfy the phase matching condition ($\Delta k = 0$), we can get the maximum of SH power.

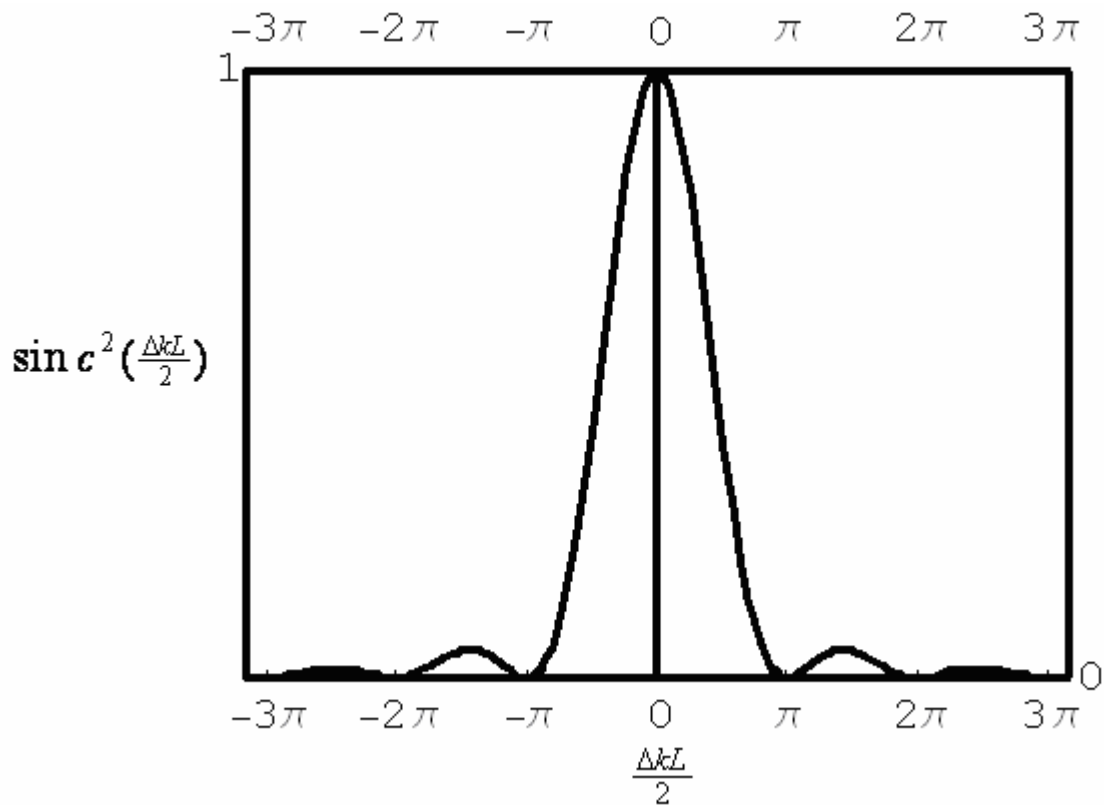


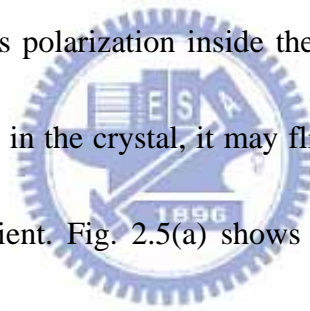
Fig. 2.4 $\sin^2\left(\frac{\Delta k L}{2}\right)$ vs $\frac{\Delta k L}{2}$.

Typically, three-wave mixing is done in a birefringent crystalline material, in which the refractive index depends on the polarization and direction of the lights that passes through. For satisfying the phase-matching condition, the polarization of the fields and the orientation of the crystal have to be chosen correctly. Such a phase-matching technique is called the angle tuning.

One undesirable effect of angle tuning is that the optical frequencies involved are not collinear with each other. This is due to the fact that the extraordinary wave propagating through a birefringent crystal possesses a Poynting vector which is not parallel with the propagation vector (critical phase-matching). This would lead to the beam walkoff which limits the nonlinear optical conversion efficiency.

Another phase-matching technique is called temperature tuning. The crystal is controlled at a certain temperature to achieve the phase matching condition. Beam walkoff is avoided by forcing all frequencies to propagate at the angle 90° with respect to the optical axis of the crystal(non-critical phase-matching).

Quasi-phase matching scheme allows the choice of the largest nonlinear coefficient with non-critical phase-matching. To obtain a quasi-phase matching structure, one may periodically modulate the nonlinear coefficient by altering the crystal symmetry in the nonlinear optical material. A class of materials called ferroelectric crystal (such as lithium niobate and lithium tantalate) possesses a spontaneous polarization inside the crystal. If one applies an external field larger than the intrinsic field in the crystal, it may flip the crystal symmetry and change the sign of the nonlinear coefficient. Fig. 2.5(a) shows the periodic structure, the relation between the SH intensity and the interaction length for ferroelectric crystals, and Fig. 2.5(b) also shows the periodic structure, the relation between the SH intensity and the interaction length for thermally poled silica fibers as a comparison.



From the Fourier expansion, the periodically modulated second-order nonlinearity $d(z)$ can be written as

$$d_{eff}(z) = d_{eff} g(z) = d_{eff} \left[\sum_{m=-\infty}^{+\infty} G_m e^{-ik_m z} \right] \quad (2.29)$$

where $k_m = \frac{2\pi m}{\Lambda}$ is the periodically modulated grating wave vector, Λ is the modulated period and G_m is the Fourier coefficient.

From equation (2.29), we have

$$d_{eff}(z)e^{i\Delta kz} = d_{eff} \left[\sum_{m=-\infty}^{+\infty} G_m e^{-ik_m z} \right] e^{i\Delta kz} \quad (2.30)$$

When $k_m = \Delta k$, we can get the quasi-phase matching. The modulated period is

$$\Lambda = m \frac{2\pi}{\Delta k} = 2ml_c, \text{ where the coherent length is } l_c = \frac{\pi}{\Delta k} = \frac{\lambda_\omega}{4(n_{2\omega} - n_\omega)}.$$

For periodically poled lithium niobate, assuming the duty cycle of the modulated $d_{eff}(z)$ is 50% ($D = \frac{l}{\Lambda} = 50\%$, where l is the length of second-order nonlinearity) and the

second-order nonlinearity is a constant, then the Fourier coefficient can be calculated to be

$$G_m = \frac{2}{m\pi} \sin(m\pi D) \quad (2.31)$$

where m is the order of quasi-phase matching. In this way, the effective nonlinearity of quasi-phase matching structure is

$$d_{QPM} = d_{eff} G_m \quad (2.32)$$

For 1st order quasi-phase matching, because it is a (1,-1) type quasi-phase matching, and the effective second-order nonlinearity is

$$d_{QPM} = \frac{2}{\pi} d_{eff} \quad (2.33)$$

On the other hand, the quasi-phase matching structure of periodically poled optical fiber is (1,0) type. The effective second-order nonlinearity is thus

$$d_{QPM} = d_{eff} \frac{G_m}{2} \quad (2.34)$$

Or equivalently,

$$d_{QPM} = \frac{d_{eff}}{\pi} \quad (2.35)$$

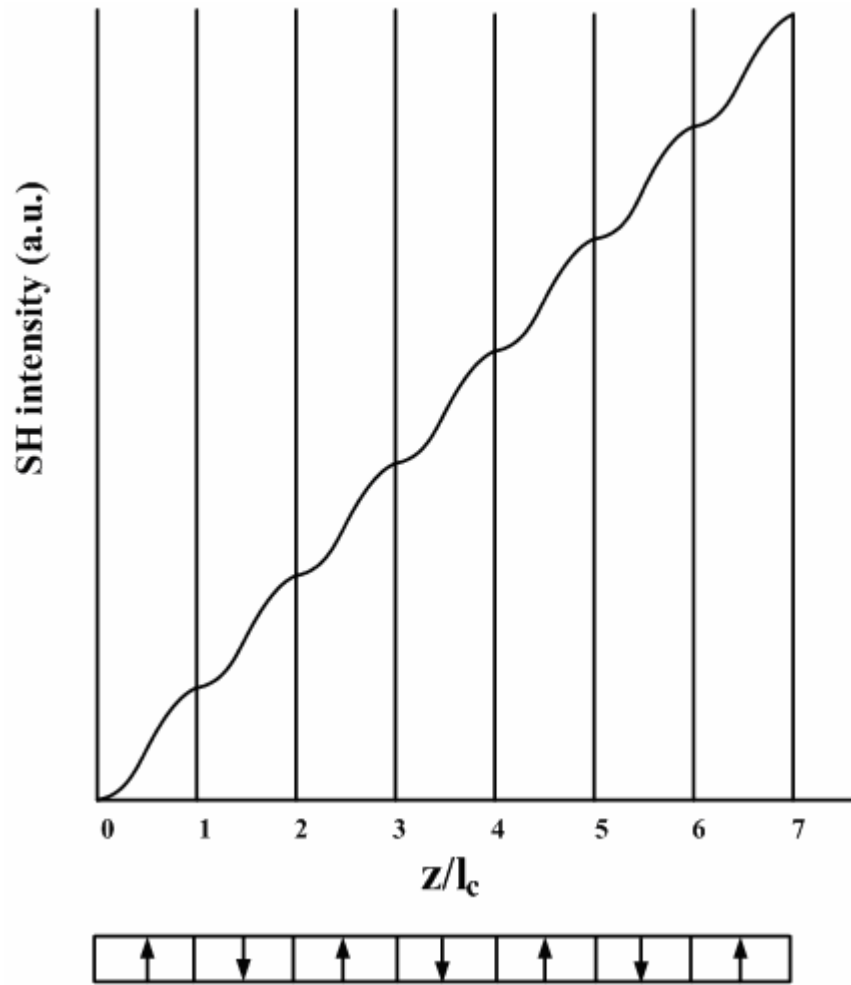


Fig. 2.5 (a) First-order quasi-phase matching of ferroelectric crystal

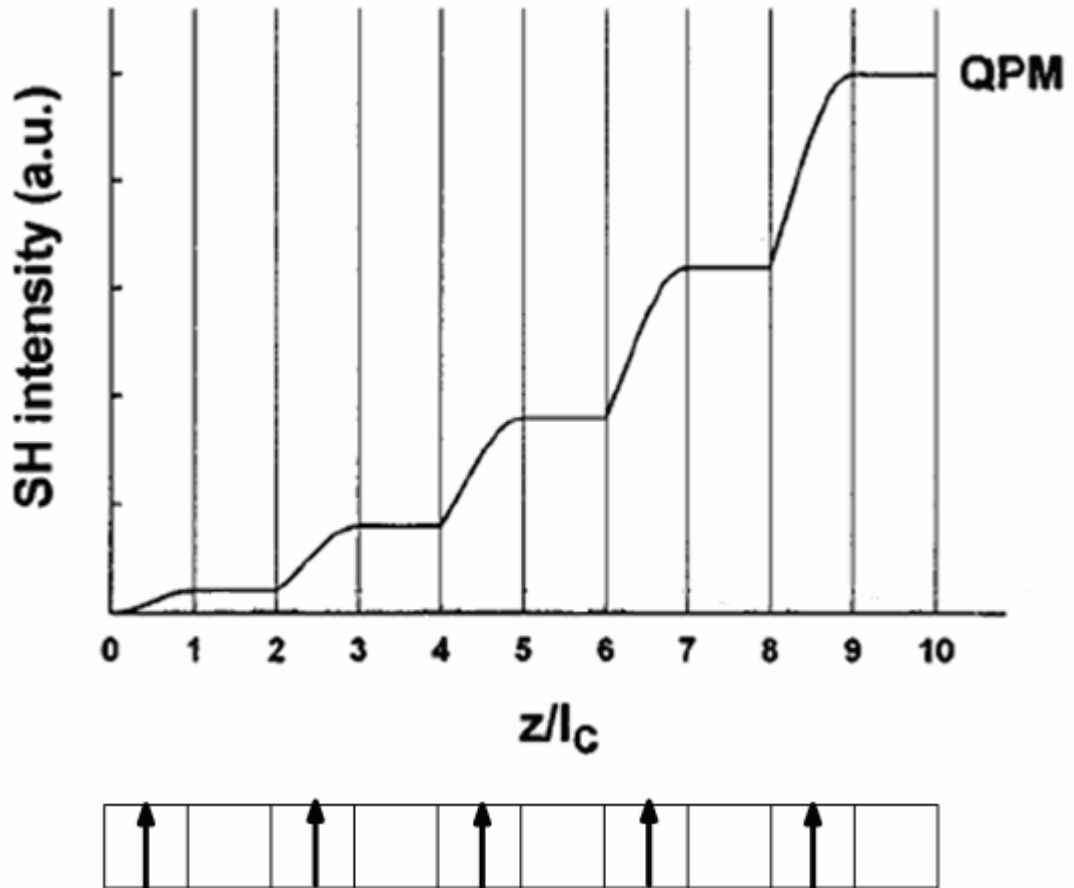


Fig. 2.5 (b) First-order quasi-phase matching of thermally poled silica fiber

2.2 Quasi-phase-matched second-harmonic generation in periodically poled fibers

The modulation for the second-order nonlinearity in thermally poled is the type $(1, 0)$, which is different from ferroelectric crystal. Quasi-phase matching occurs when the period Λ for the modulation of the nonlinear coefficient d is a multiple integer of $2l_c$, where l_c is the coherent length. The unpoled sections permit free evolution of the interacting fields without energy exchange and their relative phase shift due to propagation can compensate the phase mismatch, in the previous half period for the continuing growth of the SH intensity.

The QPM SHG in thermally poled optical fibers is different from the thermally poled glass. The quasi-phase matching waveguide condition establishes the dependence of the period Λ as a function of the fundamental wavelength (λ_ω), core radius (a) and numerical aperture (NA) [17, 18],

$$\Lambda = \frac{\lambda}{2[n_{eff,2\omega}(\lambda_\omega, a, NA) - n_{eff,\omega}(\lambda_\omega, a, NA)]} \quad (2.36)$$

where $n_{eff,2\omega}$ and $n_{eff,\omega}$ are the effective refractive indices at the SH wavelength and fundamental wavelength respectively.

For the quasi-phase matching waveguide geometry with a low fundamental light depletion, the SH power $P_{2\omega}$ is given by

$$P_{2\omega} = \frac{8\omega^2 d_{eff}^2}{n_{eff,\omega}^2 n_{eff,2\omega} \epsilon_0 c_0^3} \frac{P_\omega^2}{A_{OVL}} \frac{1}{\Delta\beta} \sin^2\left(\frac{\Delta\beta L}{2}\right) \rho \quad (2.37)$$

where $P_{2\omega}$ is the fundamental power, d_{eff} is the nonlinear coefficient which includes the overlap factor between the poled region and the interacting modes as well as the $\frac{1}{m\pi}$

reduction factor associated with the m^{th} -order quasi-phase matching. L is the length of the

periodical poled region, $A_{OVL} = \frac{1}{I_{OVL}^2}$ is an equivalent area that depends on the overlap factor

I_{OVL} between the interacting fields, $\Delta\beta = 2\frac{\omega}{c_0}[n_{eff,2\omega} - n_{eff,\omega}]$ is the wave-vector mismatch,

and ρ is an enhancement factor that takes account of the multimode nature of our

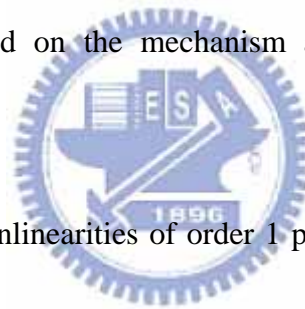
fundamental source.

Because of the large quasi-phase matching bandwidth and low group-velocity mismatch (GVM) between pulses at different frequencies in optical fibers, it allows us to use long

devices without compromising the frequency stability and is suitable for pulsed frequency conversion.

2.3 Mechanism of thermal poling

Silica optical fibers are amorphous material with macroscopic inversion symmetry and inherently have no second-order nonlinearity. In 1986, the first report of SHG in silica fibers was reported by Osterberg and Margulis [1], who discovered that prolonged exposure of fibers to infrared light causes the self-organized growth of green SH lights. Since then, wide-ranging studies are engaged on the mechanism and properties of this unexpected photoinduced phenomenon.



Since 1991, second-order nonlinearities of order 1 pm/V have been achieved in glasses using a variety of different techniques including thermal poling [4,9,10], corona poling [5] and electron implantation [6]. Here, we just discuss about the mechanism of second-order optical nonlinearity in thermally poled optical fibers.

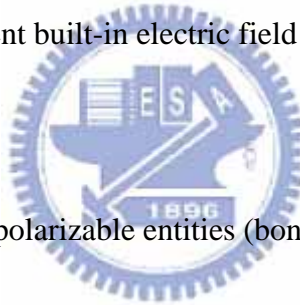
The mechanism behind the formation of second order nonlinearity in thermally poled optical fibers is not yet fully understood. Until now, there are three types of explanation for the mechanism. The first explanation is most widely used.

- (1) During the thermal poling procedure, ions such as Na^+ , H^+ , H_3O^+ or holes migrate toward the negative electrode with a relatively high mobility at a high

temperature, which leaves $\equiv Si-O^-$ in a near-surface layer contacted with the positive electrode. The ions reaching the negative electrode must be neutralized by electrons injected from the negative electrode. A high electric field arises in this region, between the negatively charged region and the anode, and this field creates second-order nonlinearity. The second-order nonlinear susceptibility $\chi^{(2)}$ is related to the third-order nonlinear susceptibility $\chi^{(3)}$ [2,4] and the relation between them is

$$\chi^{(2)} = 3\chi^{(3)}E_{dc} \quad (2.38)$$

where E_{dc} is a permanent built-in electric field induced by charge migration.



- (2) The orientation of hyperpolarizable entities (bonds or defects) in the optical fibers is realigned under the applied electric field and the formation of second-order optical nonlinearity $\chi^{(2)}$ is [19],

$$\chi^{(2)} \propto N\beta L(\rho) \quad (2.39)$$

where N is the concentration of hyperpolarizable entities, β is the second-order hyperpolarizability, and $L(\rho)$ is an orientation factor ($0 \leq L \leq 1$) under the total electric-field E within the optical fiber. L can be written as a sum of Langevin functions. $\rho = \frac{\vec{m} \cdot \vec{E}}{kT}$, where m is the dipole moment, E is the electrostatic field, T is the absolute temperature, and k is Boltzmann constant.

(3) The last explanation combines explanation (1) and explanation (2) [20], for which the effective $\chi^{(2)}$ is created via both the interaction of the intense electric field through $\chi^{(3)}$ and the dipole orientation. When the electrostatic field $E < 1$ V/nm, the dipole orientation plays the main role in the formation of $\chi^{(2)}$, whereas the interaction through $\chi^{(3)}$ is the dominant factor for larger fields. When $E > 3$ V/nm, the poling temperature must be over a threshold value, and there exists an optimal temperature. Therefore, the second-order nonlinearity from the combination of the orientation of the dipole and $\chi^{(3)}$ is

$$\chi_{333}^{(2)} = 3\chi_{3333}^{(3)}E + N\beta L_3(\rho) \quad (2.40)$$

$$\chi_{311}^{(2)} = 3\chi_{3113}^{(3)}E + 0.5N\beta[L_1(\rho) - L_3(\rho)] \quad (2.41)$$

The key factors determining the values of $\chi_{333}^{(2)}$ and $\chi_{311}^{(2)}$ are the electrostatic field E and the dipole density N in the poled region. Here $L_1(\rho)$ and $L_3(\rho)$ are the first-order and third order Langevin functions, respectively. When ρ is small, the $L_1(\rho)$ and $L_3(\rho)$ can be represented as,

$$L_1(\rho) = \frac{\int_0^\pi \cos\theta e^{\rho\cos\theta} \sin\theta d\theta}{\int_0^\pi e^{\rho\cos\theta} \sin\theta d\theta} \approx \frac{\rho}{3} \quad (2.42)$$

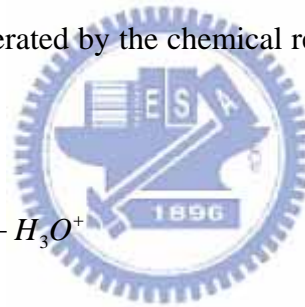
$$L_3(\rho) = \frac{\int_0^\pi \cos^3\theta e^{\rho\cos\theta} \sin\theta d\theta}{\int_0^\pi e^{\rho\cos\theta} \sin\theta d\theta} \approx \frac{\rho}{5} \quad (2.43)$$

where θ is the polar angle between the electric field E and the molecular

dipole.

Fig. 2.6 illustrates the formation process of the depletion region near the anode surface of the thermally poled fused silica [21]. Under thermal poling process, the Na^+ ions are with energies in excess of the potential barrier under the high temperature about 280°C and thus can move into the SiO_2 network. While a high dc voltage is applied, alkali metal ions (such as Na^+ ions) will drift to the cathode where most of them are neutralized by the incoming electrons, as shown in Fig. 2.6(a). If all Na^+ ions within about $5\ \mu\text{m}$ of the anode surface in the fused silica is depleted, an intense electric field E of about $10^7\ \text{V/cm}$ is established at this very thin region, and H_3O^+ is generated by the chemical reaction of $\equiv\text{Si}-\text{OH}$ with H_2O , as

described by equation (2.44),



Due to the thermal fluctuations, some of the ions will also drift to the cathode and are neutralized, as shown in Fig. 2.6(b). With both of the H_3O^+ and Na^+ ions drifting to the cathode, then $\text{Si}-\text{O}^-$ ions are left. Over there a negative space charge is generated near the anode surface, and a negative depletion layer is also formed. After that, H_3O^+ continues drifting to the cathode and the negative depletion layer slowly extends into the interior of the fused silica. Thereafter, because of the thermal fluctuations, the water molecules H_2O in the air diffuse into the fused silica and react with the fused silica network to form immobile hydroxyl (OH), $\equiv\text{Si}-\text{OH}$,



After that, $\equiv Si-OH$ react with H_2O to generate H_3O^+ under an intense electric field near the anode surface, as by equation (2.44). Then this H_3O^+ builds a positively charged layer. On the other hand, the thermal fluctuations and the intense electric field cause the fused silica to ionize, and the ionized electrons drift to anode and are neutralized, as shown in Fig. 2.6(c).

After the thermal poling process is accomplished, the maximum electric field exist in the region between the positively charged region and the negative depletion layer in the depletion region, and thus this region is most greatly ionized, as shown in Fig. 2.6(d). Fig. 2.7 (a) and Fig. 2.7 (b) show the planar schematic diagram of fused silica network before poling and after poling, respectively.

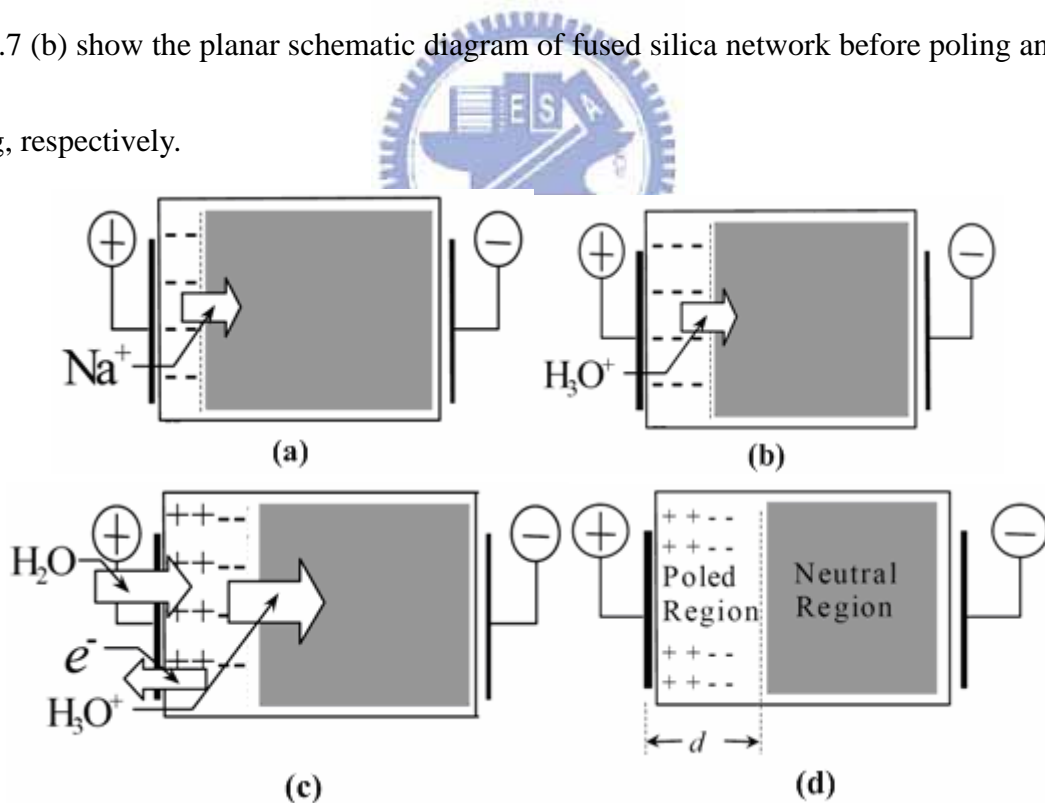


Fig.2.6 Formation process of the depletion region near the anode surface of the thermally poled fused silica

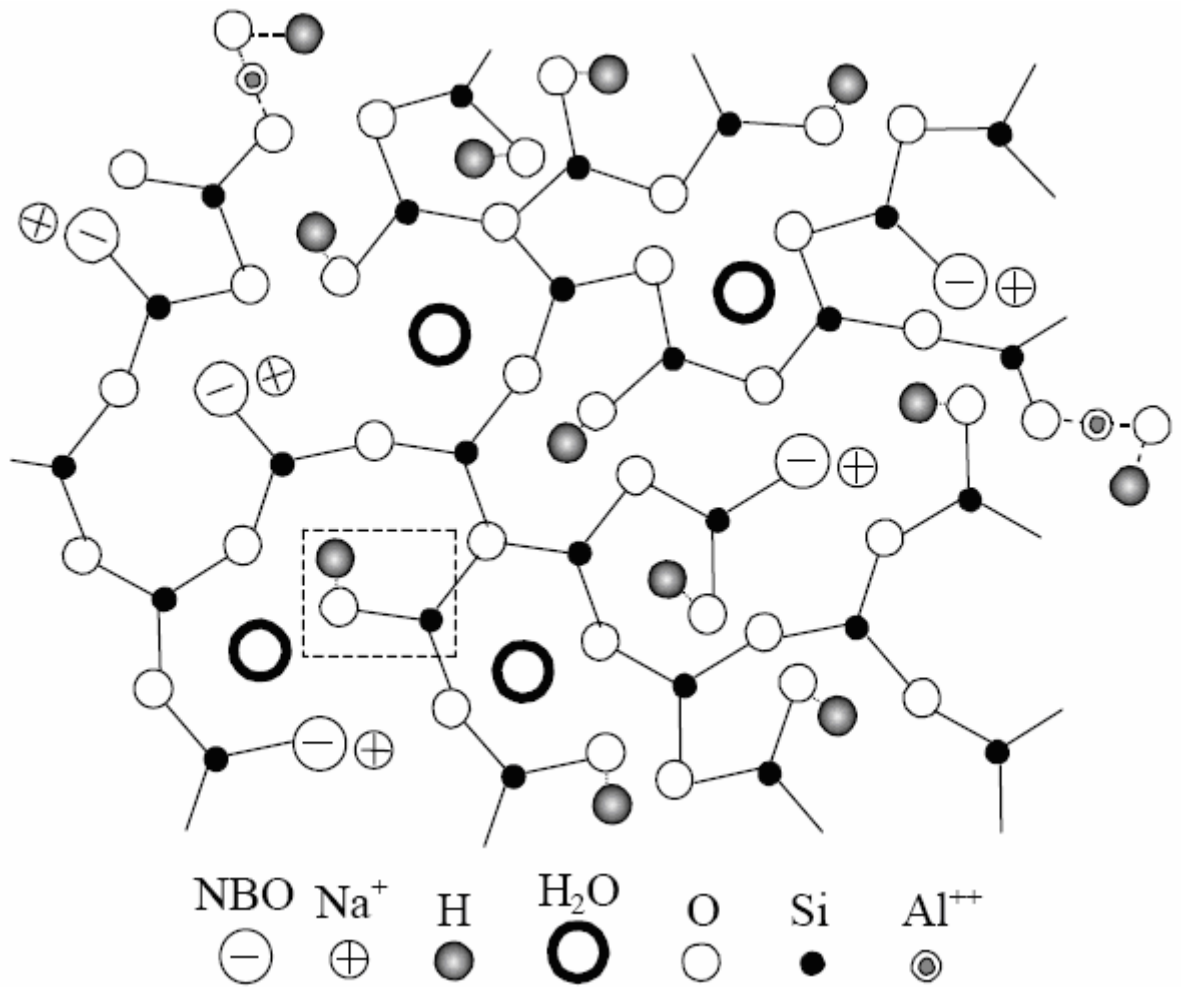


Fig. 2.7 (a) Planar schematic diagram of fused silica network before poling

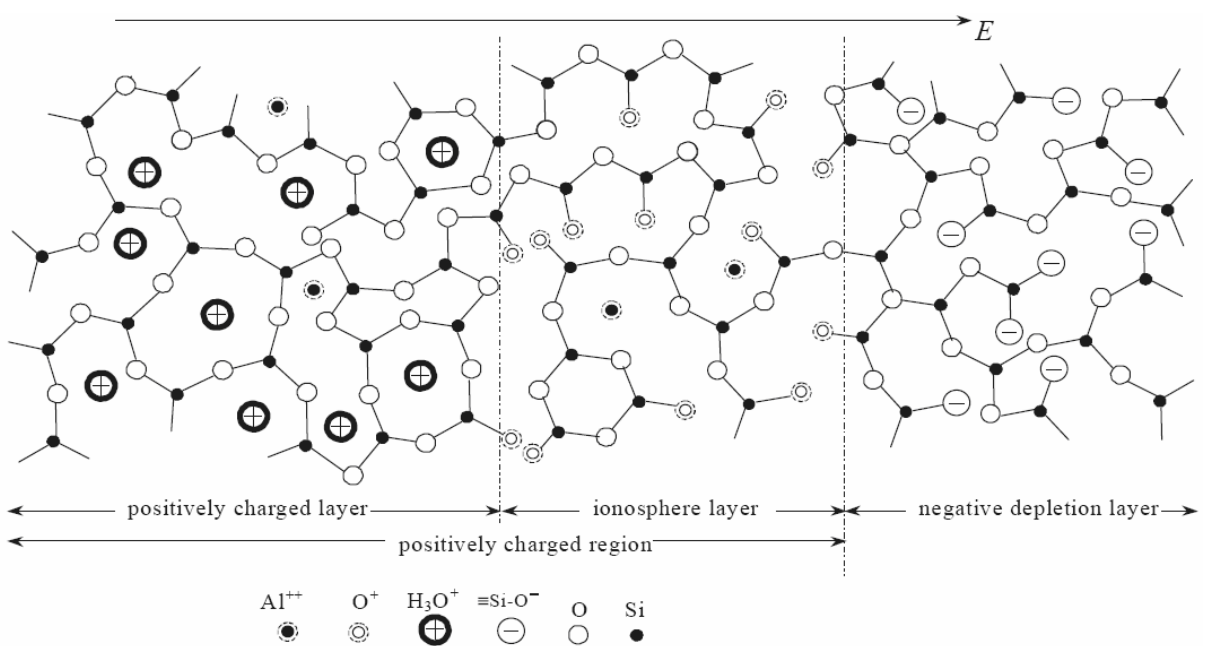
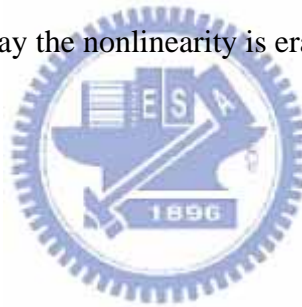


Fig. 2.7 (b) Planar schematic diagram of fused silica network after poling

2.4 Mechanism of ultraviolet erasure

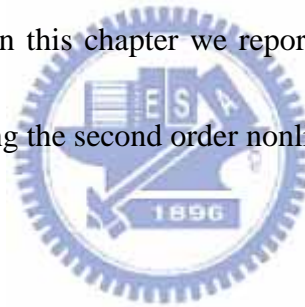
The thermally poled optical fiber can be erased by heating [2], electron beam [8], ultraviolet [9,10], or near infrared [11], which could be used to achieve the QPM SHG in optical fibers. Here, we just discuss about the UV erasure. The second-order nonlinearity in thermally poled optical fibers can be erased by UV simply because of the vanishment of the built-in electric field. When the UV lights are exposed to the thermally poled optical fiber, $\equiv Si-O^-$ is destroyed by the one-photon absorption process. Holes from the conduction band are considered to be trapped at $\equiv Si-O^-$ sites and thus the space charges of $\equiv Si-O^-$ are neutralized. In this way the nonlinearity is erased after the UV exposure.



Chapter 3 Experimental procedures and results

3.1 Introduction

Silica optical fibers are amorphous material with macroscopic inversion symmetry and inherently have no second-order nonlinearity. But in 1986, Osterberg and Margulis reported that the Ge-doped fiber irradiated by intense 1064nm laser can exhibit SHG with the SH conversion efficiency as high as 5% [1]. Later, Myers et al. found that large and stable second-order nonlinear susceptibility $\chi^{(2)}$ (~ 1 pm/V) could be created in fused silica by means of thermal poling [4]. Since then, there have been intensive researches on the poling of glass materials and glass fibers. In this chapter we report our experimental results on using D-shape optical fibers for achieving the second order nonlinearity through thermal poling.



3.2 D-shape optical fiber

In our experiment, the fibers we used were called the D-shape optical fibers. The shape of these fibers looks like a D character as shown in Fig. 3.1. The core of the D-shape fibers is in an elliptical shape and its index is higher than the surrounding cladding. The D-shape optical fibers are polarization maintaining fibers, which employ the property of geometrical birefringence to achieve the polarization preserving characteristics. The fibers are constructed of high-grade silica materials and various high purity dopants, such as germanium (Ge). This also offers significant advantages, including low loss and high polarization maintaining. Some

of the important parameters of the D-shape fibers are listed in the Table 3.1.

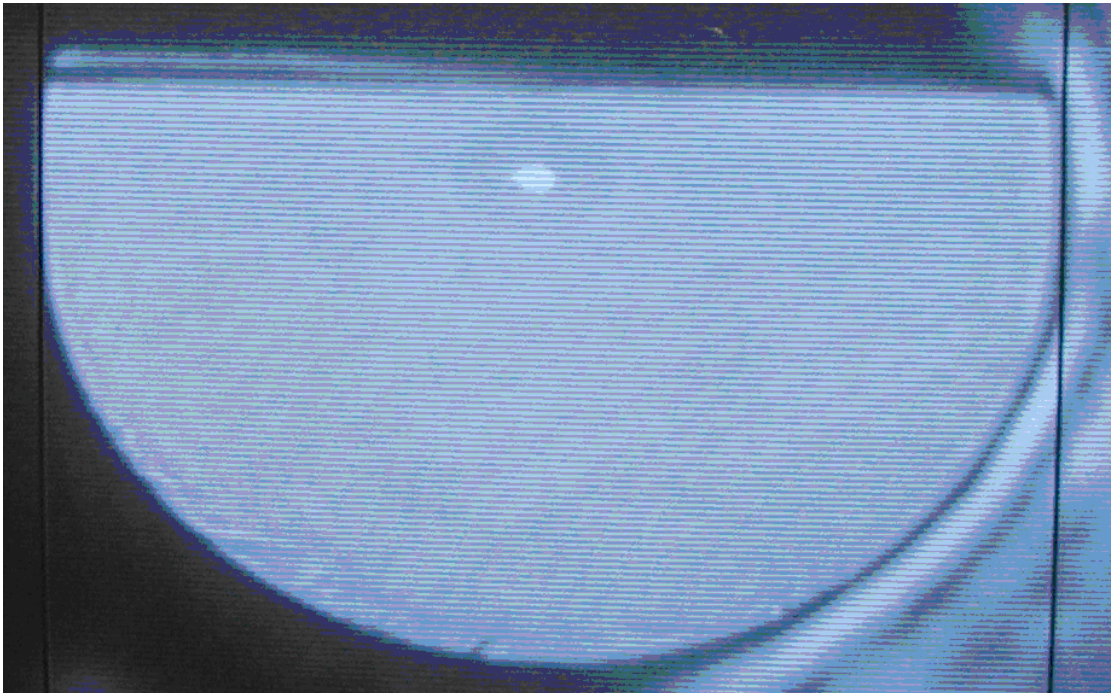


Fig. 3.1 D-shape fiber

Nominal Operating Wavelength (nm)	1550
Single Mode Operating Band (nm)	1360-1680
Cut-off Wavelength (nm)	1160±70
Attenuation, dB/km	2-5
Polarization Holding (h), dB-m	40
Normalized Birefringence	1.5×10^{-4}
Fiber Diameter (microns) ± 3	125
Center of Core to Flat (microns)	16
Coating Diameter (microns) ± 15	245

Table 3.1 The parameters of the D-shape fibers

3.3 Experimental procedures

In this section, we describe the procedure of thermal poling in optical fibers. Before the

thermal poling, we used the BOE solution ($\text{HF}:\text{NH}_4\text{F} = 1:6$) to etch the optical fibers so that the plane surface is very close to the core region.

3.3.1 Etching of D-shape fibers

The D-shape fiber used in our experiment has an outer diameter of $125\ \mu\text{m}$ and the distance between the plane surface and the core region is $16\ \mu\text{m}$. Before proceeding the thermal poling, we have to etch the fiber with the BOE solution so that the flat surface to fiber core distance is reduced to $1\ \mu\text{m}\sim 5\ \mu\text{m}$, as shown in Fig. 3.2. In this way, after poling, the nonlinear layer under the anodic surface is inside the core region. The etching rate is about $1.75\ \mu\text{m}/10\ \text{min}$.

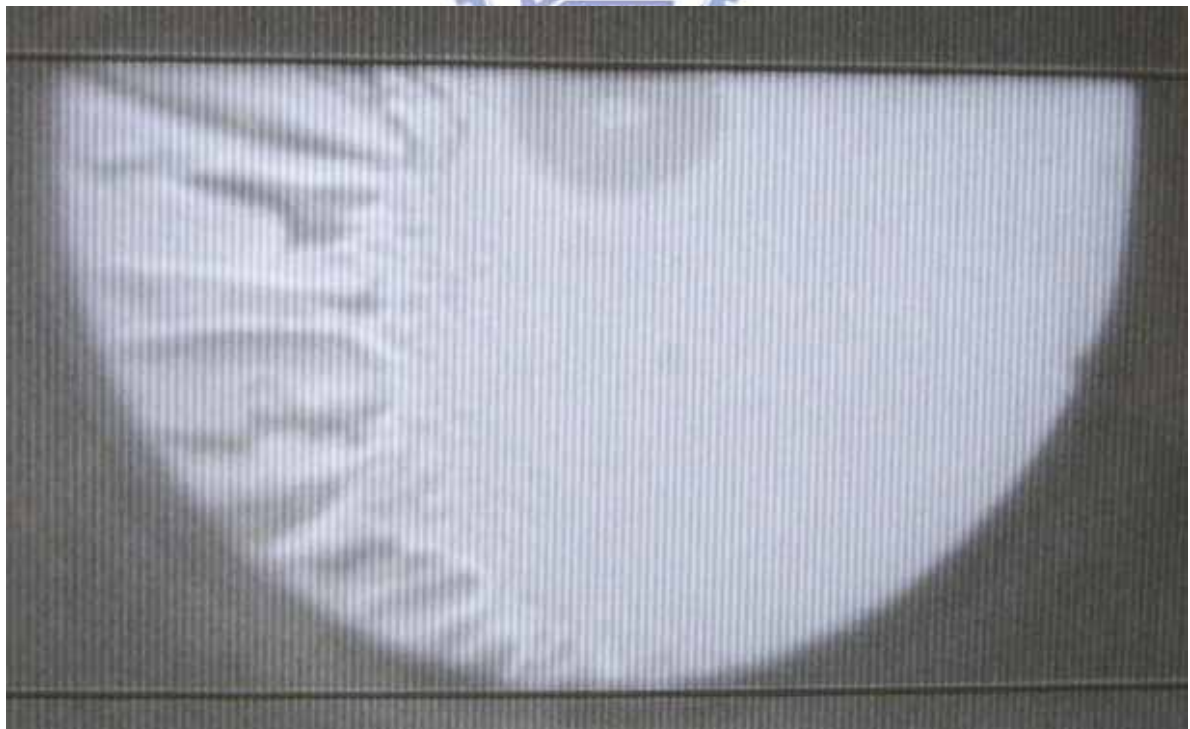
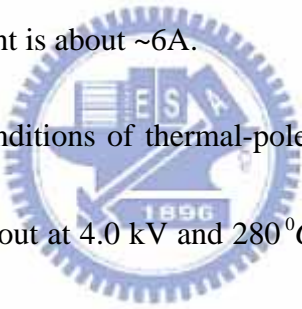


Fig. 3.2 Etched D-shape fiber

3.3.2 Thermal poling

The etched fiber was sandwiched between two electrodes with the anodic electrode on the flat surface of etched fiber. The electrodes were made by n-type {1, 0, 0} silicon wafer. One of them was placed on the fused silica plate with a dimension $20\text{ mm} \times 20\text{ mm} \times 1\text{ mm}$ (length \times wide \times depth). Fig. 3.3 shows the diagram of the thermal poling system. The temperature sensor is a K-type thermo-coupler and the maximum heating temperature is $400\text{ }^{\circ}\text{C}$, where the temperature is controlled by a temperature controller (Omega, CNi1633-c24). The heater is isolated by ceramic and its periphery is covered with thermal insulated cotton. The heating current is about $\sim 6\text{ A}$.



According to the reported conditions of thermal-poled fused silica as shown in Fig 3.4 [18], our thermal poling is carried out at 4.0 kV and $280\text{ }^{\circ}\text{C}$ for 30 minutes. The temperature is varied from the room temperature to $280\text{ }^{\circ}\text{C}$ by the heater for about 1 hour, and thereafter the electrodes are applied with a voltage of 4 kV for 30 minutes. The heater is then turned off and cooled down to room the temperature in 120 minutes with the high voltage still applied. If the applied voltage is above 4.2 kV , air breakdown is observed.

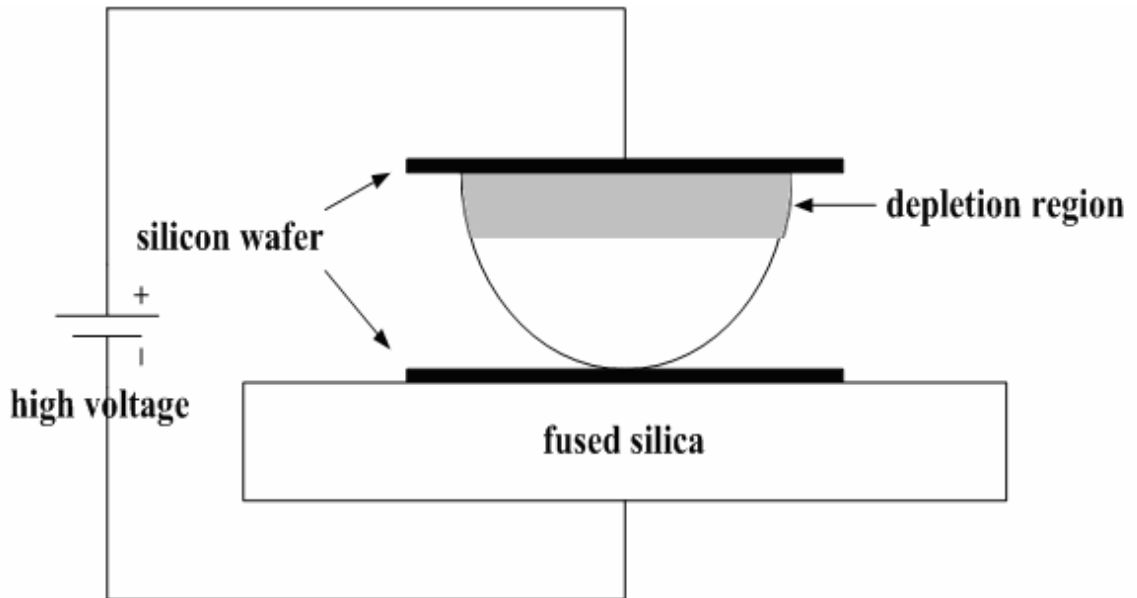


Fig. 3.3 The diagram of the thermal poling system.

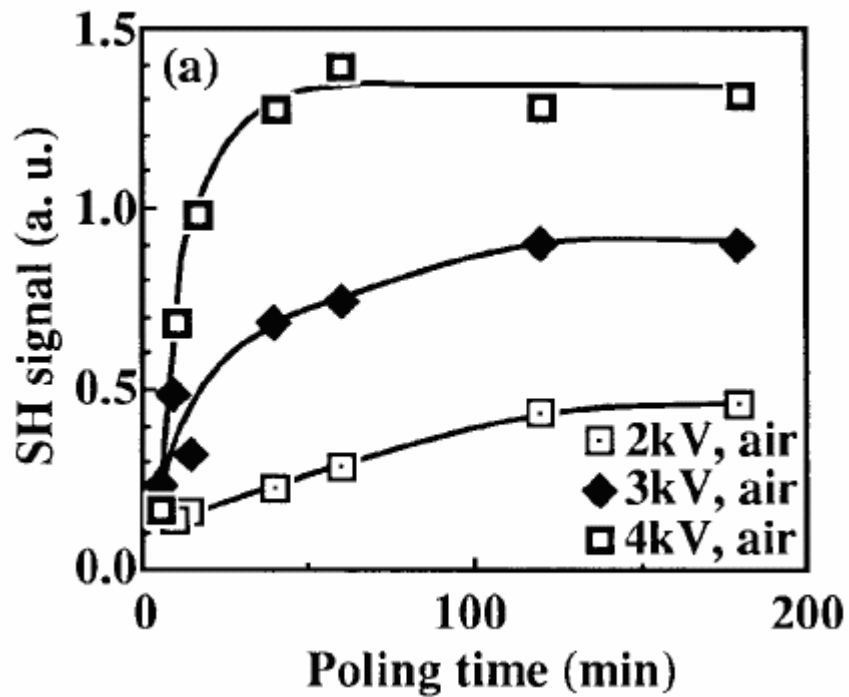


Fig 3.4 SH signal vs poling time at 280°C, in Ref. [18]

3.3.3 Second-harmonic generation measurement

In the experimental setup, a 1064 nm Nd:YAG laser is used as the light source, which is operated in a pulsed mode and has a 2kHz repetition rate with ~20 ns pulse width. An isolator

is placed after the Nd:YAG laser to reject the reflected light from optical components. After that, the light passes through a half-wave plate through which we can adjust the polarization of the laser light. After passing through a focus lens, the light is focused into an objective lens and then coupled into the thermally poled D-shape fiber.

An objective lens is placed after the end of the D-shape fiber to collimate the output light, and a dichromic mirror reflects the SH light to a 532 nm band pass filter, which can filter out the 1064 nm lights from the mixing wavelength lights. After that we use a high sensitive power detector to make the measurement. The whole experimental setup is shown in Fig. 3.5.

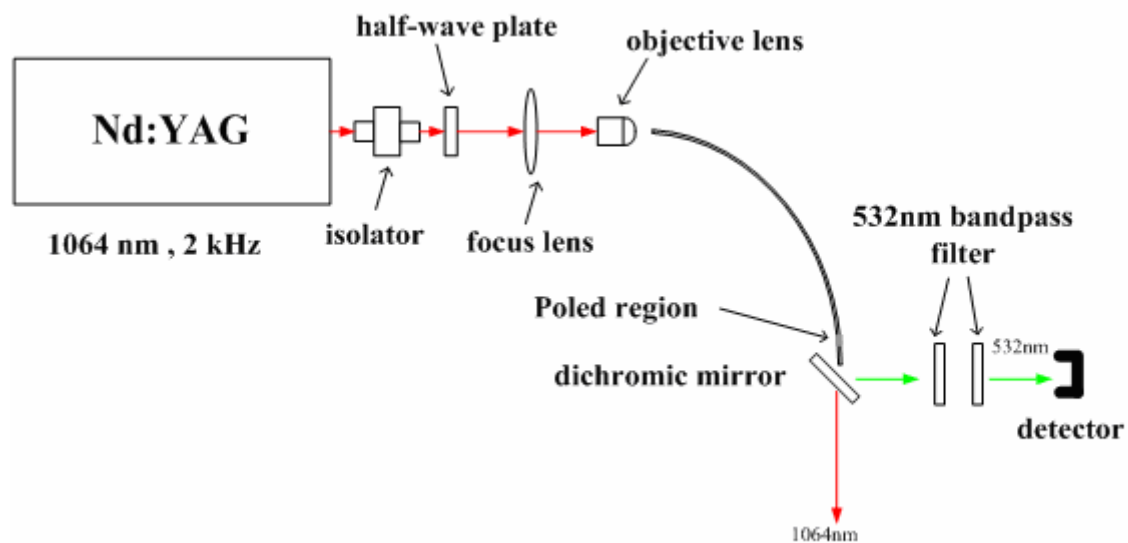
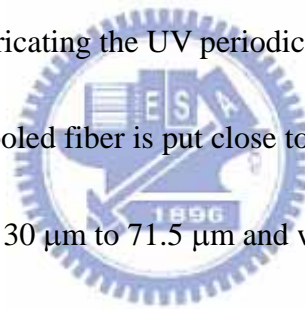


Fig. 3.5 SH measurement experimental setup

3.3.4 Ultraviolet erasure

Fig. 3.6 illustrates the UV erasure experimental setup. The pump laser was a diode-pumped Q-switched Nd:YAG laser. Its wavelength is 1064nm, the repetition rate is

4kHz and the pulse-width is about 20ns. A half-wave plate is used to adjust the polarization orientation of the 1064nm lights for optimizing the harmonic generation processes. After a focus lens, the fundamental laser beam is incident into the SHG crystal, a 3X3X5 mm³ type-II KTP, which end faces are dual antireflection coated for 1064nm and 532nm. A type-I BBO crystal with dual antireflection coating for 532nm and 266 nm is use as a second-harmonic generation crystal so that we can get 90mW of 266nm UV light from the 3.5W pump source. We use two cylindrical lenses to broaden and collimate the UV lights. The beam size of the UV light is about 8 mm (e⁻¹). A shutter is placed before the focusing lens, which is used to control the exposure time. For fabricating the UV periodic grating, the experimental setup is shown in Fig. 3.7. The thermally poled fiber is put close to the amplitude mask, which has 84 patterns with grating periods from 30 μm to 71.5 μm and with the duty cycle=50%. We can choose the suitable grating period to fabricate quasi-phase matching periodical thermally poled optical fibers.



Before choosing the grating period, we use the Sellmeier's equation of fused silica to estimate the quasi-phase matching period with difference mol% of doped GeO₂. The quasi-phase matching periods for fused silica doped with GeO₂ with different mol% are listed in Table 3.2. We observe that the quasi-phase matching period becomes shorter when the mol% of doped GeO₂ is increased.

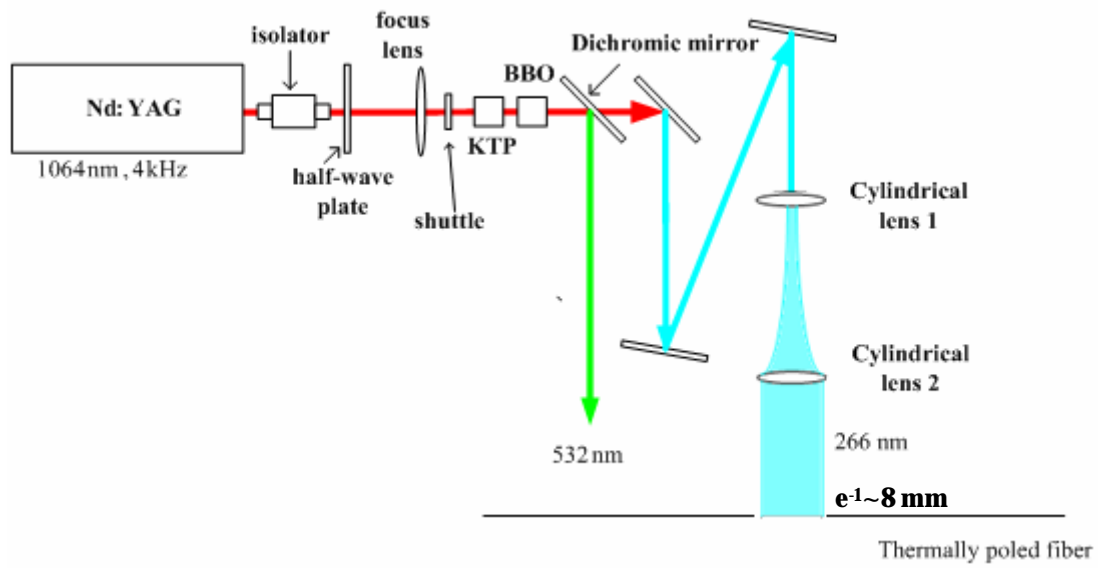


Fig.3.6 Experimental setup of UV erasure system

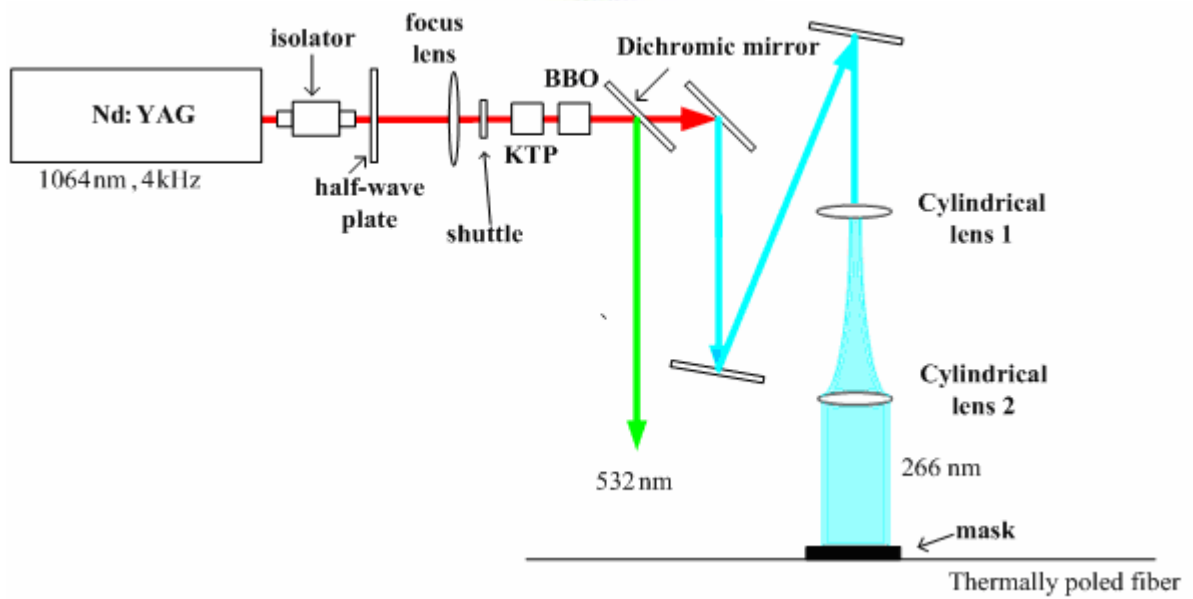


Fig. 3.7 Experimental setup of UV periodic grating

Material	Phase-matched period(μm)
Fused silica	48.114
Fused silica doped GeO_2 6.3 mol%	45.7904
Fused silica doped GeO_2 8.7 mol%	44.7474
Fused silica doped GeO_2 11.2 mol%	44.2789
Fused silica doped GeO_2 15 mol%	42.995
Fused silica doped GeO_2 19.3 mol%	41.0121

Table 3.2 Quasi- phase matching period for fused silica with difference mol% of doped GeO_2

3.4 Results and conclusion

In this section, we show the results of the pump power dependence and the polarization dependence for the SH power. Some discuss about the results are also given.



3.4.1 Thermally poled fused silica plate

In order to confirm our thermal-poling system is working, we fabricate a thermal-poled fused silica plate [22, 23]. The fused silica plate is sandwiched between the electrodes made of the n-type $\{1, 0, 0\}$ silicon wafers. The poling temperature is raised to 280°C and the 4kV voltage is applied for 60 minutes. The heater is then turned off and cooled down to room temperature in 120 minutes with the high voltage still applied. The scheme of thermally poled fused silica plate is shown in Fig. 3.8.

Because the UV lights can erase the nonlinearity of thermal-poled fused silica [9,10], we use an amplitude mask with a period about $150 \mu\text{m}$ and a phase mask with sub-micron period

for periodic UV exposure. The erasure UV source is a CW 244 nm UV light from a frequency-doubled Argon laser with 150 mW average power and 6 mm (e^{-1}) Gaussian beam size. Because the etching rate of thermally poled fused silica plate is slower than the unpoled one, after an attack of BOE solution for 10 minutes, the long and short periodic domain patterns can be seen, as shown on Fig. 3.9 (a) and Fig. 3.9(b), which are viewed under an optical microscope and an atomic force microscope (AFM) scanning, respectively.

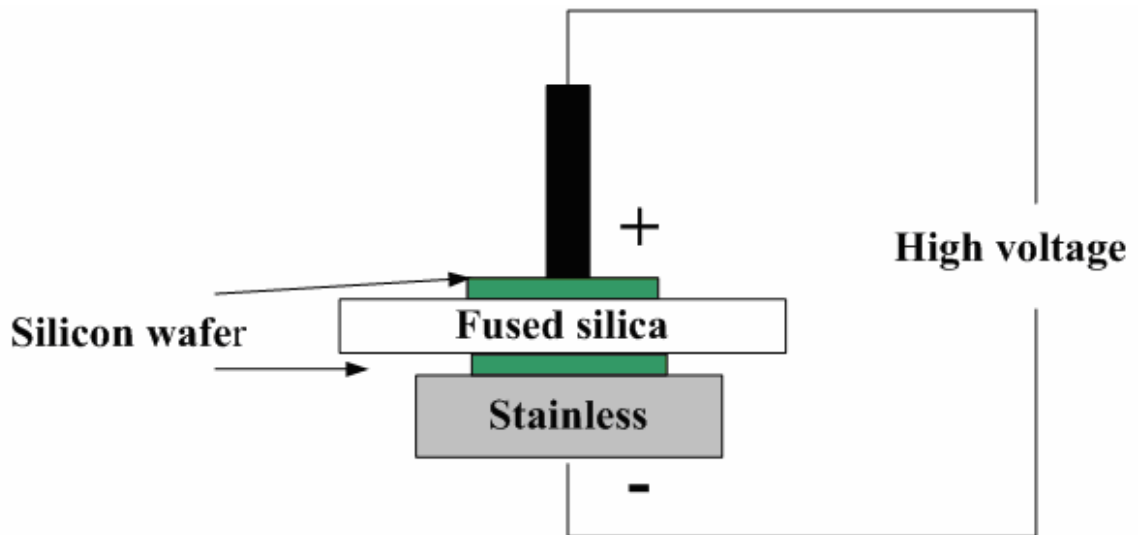


Fig. 3.8 The diagram of thermally poled fused silica plate



Fig. 3.9 (a) The surface of the etched thermally poled fused silica plate viewed under an optical microscope.

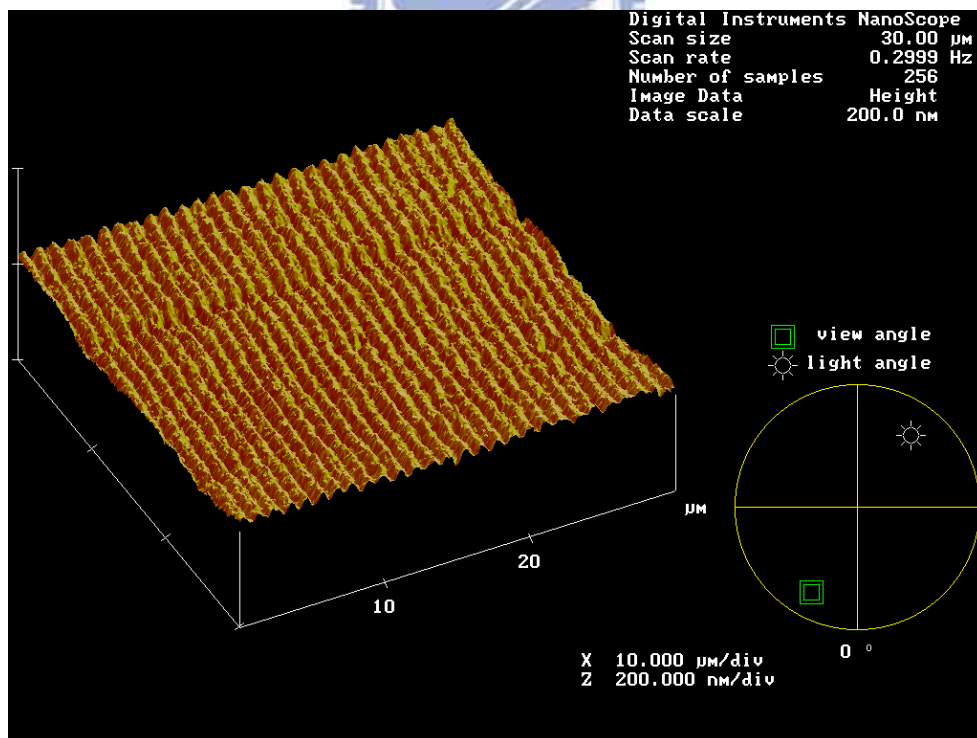


Fig. 3.9 (b) The surface of the etched thermally poled fused silica plate viewed under an AFM scanning

3.4.2 Pump power dependence for second-harmonic generation power

Fig 3.10 shows the SHG power $P_{2\omega}$ versus the fundamental pump power P_{ω} . From equation (2.28), we know that the SHG power is proportional to P_{ω}^2 . In the figure, we fitted the $S \rightarrow S$ curve with a second-order polynomial function and got the following expression:

$$P_{2\omega} = 0.77892 + -0.0679 \times P_{\omega} + 0.00278 \times P_{\omega}^2 \quad (3.1)$$

From equation (3.1), the third term in the right hand side is a quadratic function, which is the main dominant term of the equation. In this way, we verify that it is a indeed quadratic relation between the SHG power and the fundamental pump power.

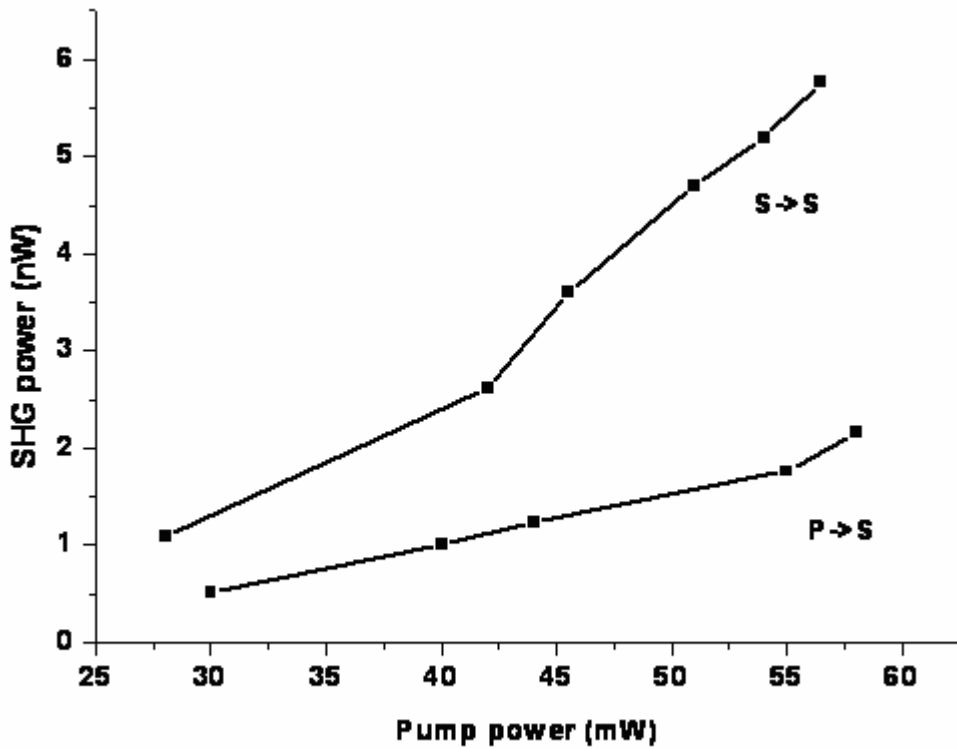


Fig. 3.10 SH power vs fundamental power for $S \rightarrow S$ and $P \rightarrow S$ conversion.

3.4.3 Polarization dependence for second-harmonic generation power

In the experiment, by tuning the angle of the half-wave plate, we found that the SHG power is changed with the tuning angle. It is because when the polarization of the fundamental laser beam is parallel to the direction of poling electric field, we can get the maximum SHG power. If the direction of the polarization is perpendicular to the direction of poling electric field, the SHG power is minimum. Fig 3.11 shows the SH power versus the tuning angle of half-wave plate.

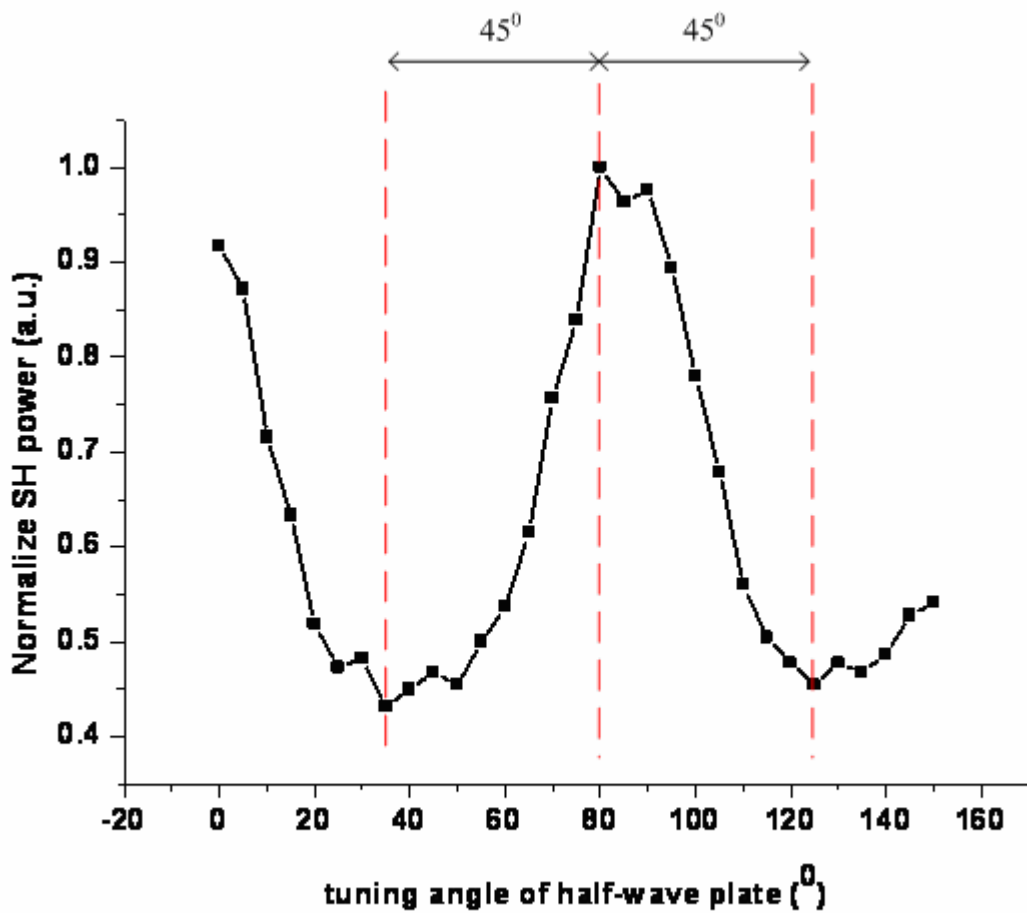


Fig. 3.11 SH power vs tuning angle of half-wave plate

3.4.4 Estimation of d_{33}

We can now roughly estimate the value of d_{33} for our thermally poled fiber based on the results from reference [7]. From the reference, the grating of the sample was 75 mm long. A peak SH power of 1.2 kW was generated from 4.0 kW peak fundamental power and the estimated d_{eff} was 0.014 pm/V. From equations (2.15) and (2.28), we know that d_{33} is equal to $3d_{31}$ and the SH power is proportional to d_{eff}^2 , L^2 and P_{ω}^2 . In our experiment, the peak SH power we get is 0.136825 mW, for which we assume that the SH pulse is of a similar duration to the fundamental pulse rather than being shorter (the reduction factor would be $\sqrt{2}$) and the peak fundamental power is 1.35 kW. After the calculation, we estimate the d_{33} for our thermally poled fibers should be about 0.023 pm/V.

3.4.5 UV erasure and UV periodic grating

In order to achieve QPM, we try to use UV erasure method to fabricate the second nonlinearity grating. We first fabricate a thermally poled fiber of which the poled region is 6 mm long we then exposed the poled region to the UV lights with the beam size of 8 mm (e^{-1}) to erase the second-order nonlinearity in the fiber. We observe that when the fiber is exposed for 10 minutes, the second-order nonlinearity in the fiber is totally erased.

We have also tried to fabricate periodic grating in the fiber with different periods of amplitude masks. Unfortunately so far we have not been able to observe the quasi-phase matching effect in the fabricated fiber devices. It may be due to the incorrect grating period

we use such that the phase-matched wavelength is not close enough to the 1064 nm.



Chapter 4 Conclusions

4.1 Summary of results

We have successfully induced second-order nonlinearity in optical fibers by means of the thermal poling technique. From the SHG measurement, we observe that the SH power is proportional to the square of the fundamental pump power and the SH power generate from d_{31} is lower than the SH power generate from d_{33} . These observations agree with the expectation from the principles of nonlinear optics. We also observe that the SH power is varied by tuning the angle of the half-wave plate. This is conform to the characteristics of the half-wave plate, for which if the polarization of the incident light makes an angle with the axis of the half-wave plate, the polarization of the laser light rotates by an angle -2 . We thus observe that the maximum and the minimum SH powers occur at angles that differ by 45° . The rough estimation of the achieved d_{33} is about 0.023 pm/V . By the UV erasure and BOE solution etching, we can obtain the periodic pattern on the surface of thermally poled fused silica plate. It confirms that the UV erasure method should be applicable in fabricating QPM SHG devices in optical fibers. Finally, we observe that the second-order nonlinearity in thermally poled optical fiber can be totally erased by the UV erasure of 10 minutes.

4.2 Future work

The final goal of this study is to fabricate poled QPM fiber devices. Because of the low

dispersion and low group-velocity mismatch possibly achieved in optical fibers, the relatively low value of the nonlinear coefficient can be compensated by an increase in the length of the poled fiber and by the technique of QPM. Poled QPM optical fibers also can be used for the generation of entangled photon-pairs by parametric down-conversion, which can be useful for achieving all-fiber quantum information applications. Due to the incorrect grating period we use, we have not observed the QPM effects so far. In the future we will continue to actually fabricate poled QPM fiber devices and to explore their applications.



References

- [1] U. Osterberg and W. Margulis, "Dye laser pumped by Nd:YAG laser pulses frequency doubled in glass optical fiber", *Opt. Lett.*, vol. 11, pp. 516-518, 1986
- [2] R. H. Stolen and H. W. K. Tom, "Self-organized harmonic generation in optical fibers", *Opt. Lett.*, vol. 12, pp. 585-587, 1987
- [3] M. -V. Bergot, M. C. Farries, M. E. Fermann, L. Li, J. Poyntz-Wright, P. St. J. Russell, and A. Smithson, "Generation of permanent optically induced second-order nonlinearities in optical fibers by poling", *Opt. Lett.*, vol. 13, pp. 592-594, 1988
- [4] R. A. Myers, N. Mukherjee, and S. R. J. Brueck, "Large second-order nonlinearities in poled fused silica", *Opt. Lett.*, vol. 16, pp. 1732-1734, 1991
- [5] A. Okada, K. Ishii, K. Mito, and K. Sasaki, "Phase-matched second-harmonic generation in novel corona poled glass waveguides", *Appl. Phys. Lett.*, vol. 60, pp. 2853-2855, 1992
- [6] P. G. Kazansky, A. Kamal, and P. St. J. Russell, "High second-order nonlinearities induced in lead silicate glass by electron-beam irradiation", *Opt. Lett.*, vol. 18, pp. 693-695, 1993
- [7] V. Pruneri, G. Bonfrate, P. G. Kazansky, D. J. Richardson, N. G. Broderick, J. P. de Sandro, C. Simonneau, P. Vidakovic, and J. A. Levenson, "Greater than 20%-efficient frequency doubling of 1532-nm nanosecond pulses in quasi-phase-matched germanosilicate optical fibers", *Opt. Lett.*, vol. 24, pp. 208-210, 1999

- [8] P. G. Kazansky, A. Kamal, and P. St. J. Russell, "Erasure of thermally poled second-order nonlinearity in fused silica by electron implantation", *Opt. Lett.*, vol. 18, pp. 1141-1143, 1993
- [9] Akihiro Kameyama, Atsushi Yokotani, and Kou Kurosawa, "Identification of defects associated with second-order optical nonlinearity in thermally poled high-purity silica glasses", *J. Appl. Phys.*, vol.89, pp.4707-4713, 2001
- [10] Akihiro Kameyama, Atsushi Yokotani, and Kou Kurosawa, "Generation and erasure of second-order optical nonlinearities in thermally poled silica glasses by control of point defects", *J. Opt. Soc. Am. B*, vol. 19, pp. 2376-2383, 2002
- [11] S. Montant, A. Le Calvez, E. Freysz, A. Ducasse, V. Nazabal, E. Fargin, and G. Le Flem, "Light-controlled erasure of induced $\chi^{(2)}$ in thermally poled glasses", *Appl. Phys. Lett.*, vol. 74, pp. 2623-2625, 1999
- [12] G. Bonfrate, V. Pruneri, and P. G. Kazansky, "Periodic UV erasure of the nonlinearity for quasi-phase-matching in optical fibers", *Conference on Lasers and Electro-Optics (CLEO)*, paper CM05, 2000
- [13] T. H. Maiman, "Stimulated Optical Radiation in Ruby", *Nature*, vol. 187, pp. 493-494, 1960
- [14] P. A. Franken, A. E. Hill, C. W. Peters, and G. Weinreich, "Generation of optical harmonics", *Phys. Rev. Lett.*, vol. 7, pp. 118-120, 1961

- [15] Robert W. Boyd, "Nonlinear Optics", Academic Press, INC., 1992
- [16] B. E. A. Saleh and M. C. Teich, "Fundamentals of photonics", John Wiley & sons, INC., 1991
- [17] Peter G. Kazansky and V. Pruneri, "Electric-field poling of quasi-phase-matched optical fibers", J. Opt. Soc. Am. B, vol.14, pp.3170-3179, 1997
- [18] Peter G. Kazansky, Philip St. J. Russell, and Hiromichi Takebe, "Glass fiber poling and applications", J. L. Tech., vol. 15, pp. 1484-1493, 1997
- [19] A. Le Calvez, E. Freysy, and A. Ducasse, "Experimental study of the origin of the second-order nonlinearities induced in thermally poled fused silica", Opt. Lett., vol. 22, pp. 1547-1549, 1997
- [20] Xueming Liu and Hanyi Zhang, "Mechanism analysis of thermally/electric field poling in fused silica", Jpn. J. Appl. Phys., vol. 41, pp. 2958-2961, 2002
- [21] Xue-Ming Liu and Ming-De Zhang, "Theoretical study for thermal/electric field poling of fused silica", Jpn. J. Appl. Phys., vol. 40, pp. 4069-4076, 2001
- [22] Huai-Yi Chen, Jin-Sheng Sue, Yi-Hsuan Lin, and Shiuh Chao, "Quasi-phase-matched second-harmonic generation in ultraviolet-assisted periodically poled planar fused silica", Opt. Lett., vol. 28, pp. 917-919, 2003
- [23] Huai-Yi Chen, Jin-Sheng Sue, Yi-Hsuan Lin, Chin-Shun Tsai, Pao-Tung Wu, and Shiuh Chao, "Thermal poling and ultraviolet erasure characteristics of type-III ultraviolet-grade

fused silica and application to periodic poling on planar substrates”, J. Appl. Phys., vol. 94, pp. 1531-1538, 2003

